NOTICE

AVIS

Canada

University of Alberta

Crack Growth Retardation by Carbon Fibre Composite Patching:
An Application to Steel Pressure Vessel Repair

by

Pamela D. Roberts

A thesis submitted to the Faculty of Graduate Studies and Research in partial
fulfilment of the requirements for the degree of Master of Science

Department of Mechanical Engineering

Edmonton, Alberta
Spring 1995

National Library
of Canada

Bibliothèque nationale
du Canada

Acquisitions and
Bibliographic Services Branch

Direction des acquisitions et
des services bibliographiques

395 Wellington Street
Ottawa, Ontario
K1A 0N4

395, rue Wellington
Ottawa (Ontario)
K1A 0N4

THE AUTHOR HAS GRANTED AN
IRREVOCABLE NON-EXCLUSIVE
LICENCE ALLOWING THE NATIONAL
LIBRARY OF CANADA TO
REPRODUCE, LOAN, DISTRIBUTE OR
SELL COPIES OF HIS/HER THESIS BY
ANY MEANS AND IN ANY FORM OR
FORMAT, MAKING THIS THESIS
AVAILABLE TO INTERESTED
PERSONS.

L'AUTEUR A ACCORDE UNE LICENCE
IRREVOCABLE ET NON EXCLUSIVE
PERMETTANT A LA BIBLIOTHEQUE
NATIONALE DU CANADA DE
REPRODUIRE, PRETER, DISTRIBUER
OU VENDRE DES COPIES DE SA
THESE DE QUELQUE MANIERE ET
SOUS QUELQUE FORME QUE CE SOIT
POUR METTRE DES EXEMPLAIRES DE
CETTE THESE A LA DISPOSITION DES
PERSONNE INTERESSEES.

THE AUTHOR RETAINS OWNERSHIP
OF THE COPYRIGHT IN HIS/HER
THESIS. NEITHER THE THESIS NOR
SUBSTANTIAL EXTRACTS FROM IT
MAY BE PRINTED OR OTHERWISE
REPRODUCED WITHOUT HIS/HER
PERMISSION.

L'AUTEUR CONSERVE LA PROPRIETE
DU DROIT D'AUTEUR QUI PROTEGE
SA THESE. NI LA THESE NI DES
EXTRAITS SUBSTANTIELS DE CELLE-
CI NE DOIVENT ETRE IMPRIMES OU
AUTREMENT REPRODUITS SANS SON
AUTORISATION.

ISBN 0-612-06577-4

Canadä

University of Alberta

Library Release Form

Name of Author: Pamela D. Roberts

Title of Thesis: Crack Growth Retardation by Carbon Fibre Composite Patching: An Application to Steel Pressure Vessel Repair

Degree: Master of Science

Year this Degree Granted: 1995

Pamela Roberts

4410-52 Street
Camrose, Alberta
T6V 1T7

Date: *April 20/95*
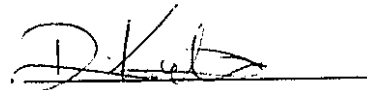
University of Alberta

Faculty of Graduate Studies and Research
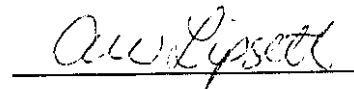
The undersigned certify that they have read, and recommend to the Faculty of Graduate Studies and Research for acceptance, a thesis entitled **Crack Growth Retardation by Carbon Fibre Composite Patching: An Application to Steel Pressure Vessel Repair** submitted by **Pamela Roberts** in partial fulfilment of the requirements for the degree of **Master of Science.**
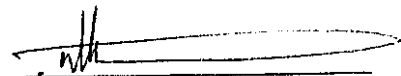
Dr. F. Ellyin

Dr. D. Kujawski

Dr. A.W. Lipsett

Dr. U. Sundararaj

Date: 95-04-19

Abstract

This study explores, experimentally, the possibility of repairing a cracked steel pressure vessel by bonding a carbon fibre composite patch over top of the damage.

The patch was fabricated from a room-temperature curing carbon fibre composite and bonded to the steel with an epoxy adhesive. The material properties of the composite patch were determined as a function of the lay up sequence and cure temperature. The shear strength of the adhesive bond was measured as a function of the patch overlap length, the patch stiffness, and the surface preparation and thickness of the steel.

Standard Compact Tension (CT) specimens were used to quantify the effect a repair has on crack growth in a steel structure. A patch was bonded to a cracked CT specimen, the specimen was subjected to cyclic loading, and the crack growth was monitored. This test demonstrated that the patch had an effect on the threshold stress intensity factor range, ΔK_{th}, and the growth of the crack in the Paris Regime. Repairs using both stop-hole drilling and patching provided a more efficient repair for the damaged CT specimens. In both repair cases, the debonding of the patch from the steel structure was monitored. Cracked biaxial specimens were used to study the feasibility of repairing a pressurized vessel. The biaxial specimens were repaired and subjected to pressure and biaxial loading.

This method of repair has shown to be effective at retarding the crack growth in cracked steel structures and has the potential to significantly prolong the operating life of vessels.

Acknowledgement

The author would like to acknowledge her supervisor,
Dr. F. Ellyin,
for his support and guidance in this project.

Table of Contents

Page

Table of Contents

Table of Contents

List of Figures

List of Figures

List of Figures

List of Tables

1.1   INTRODUCTION

All structural components contain defects. Under monotonic or cyclic loading, these defects can grow to a level which may require repair. In pressure vessels, with traditional repairing techniques, the cracks are removed by grinding operations and then welding processes are employed to replace the displaced material. The welding operation, however, has certain disadvantages, eg. embrittlement of the zone surrounding the weld, thus, making this site a likely location for crack initiation. The use of a carbon fibre composite patch has certain advantages: (1) the patch does not introduce stress concentrations or alter the quality of the steel, (2) the patch can be easily manufactured to match the contour of the pressure vessel's surface, (3) the patch is thin and therefore does not effect the geometry of the vessel significantly.

This investigation explores, using experimental investigations, the possibility of repairing a cracked pressure vessel with a carbon fibre patch in order to extend the fatigue life of the vessel.

1.2   PREVIOUS WORK

1.2.1   Patching Applications in the Aircraft Industry

The concept of patching to repair structural components is not new. The use of composite patches to repair cracks in aircraft components is a significant and accepted technology in the aircraft industry [1.1]. For example, Ong et al. [1.2] studied the use of carbon/epoxy and boron/epoxy composite patches to repair the cracks in the load bearing upper longeron in aircraft structures; many of the repaired aircraft have been in service without failure for more than 700 hours. Ong and Shen [1.3] repaired the nosedome of a composite aircraft structure using a boron/epoxy patch which kept the

structure servicing successfully for more than one year. Other such successes have also been reported [1.4,1.5].

Designing the patch, however, to effectively repair a damaged aircraft structure is not simple. Because of the complex load patterns found in a cracked structure with an applied patch, a simple analysis to determine load transfer to the patch and reduced stress intensity at the crack tip is unavailable. Intricate analysis of loads in a patched structure requires the use of a numerical investigation such as a finite element analysis [1.2,1.6]. With numerical analysis, parameters such as the reduction in the stress intensity at the crack tip, the stress concentration in the fibres at the crack, and the shear stress concentrations in the adhesive layer can be determined.

Analytical work has also been employed to design a patch. Analytical work, unfortunately, is limited by the complexity of modelling each component of the bonded structure. Rose [1.7] developed an analytical model of a patched crack by assuming that the constituents that made up the bonded assembly were both isotropic and elastic and by assuming that the adhesive layer could be modelled as a shear spring. Baker [1.5] outlines a design approach to fabricate a minimum thickness patch which will not exceed the available overlap length and will not fail under applied loads. Baker's design approach is based on analytical analysis to determine the design parameters.

Whether they be experimental, analytical, or numerical analysis, previous investigations of patching cracked aluminum aircraft components concluded that patching a damaged structural component increases the component's fatigue life.

1.2.2   Patching Applications in the Pressure Vessel Industry

Patching of cracked steel has also been investigated but not as extensively as the patch

repair of aluminum aircraft structures. Alawi and Saleh [1.8] bonded a steel patch to a cracked steel specimen and observed that the growth rate of the crack in the patched steel structure was reduced over that of the unpatched case. Hu et al. [1.9] investigated the effectiveness of using a steel patch bonded with an epoxy resin over a crack in a damaged steel pressure vessel. They discovered that the steel patch was effective in increasing both the static ultimate strength of a pressure vessel with a through-thickness crack and the fatigue life of a pressure vessel with a part-through crack. These investigations infer that the repair of pressure vessels is feasible using a bonded patch. To the author's knowledge, however, there has been no research done on the repair of cracked pressure vessels using carbon fibre composite patches.

1.3 DETAILS OF THIS WORK

Whereas there has been extensive investigations in the patch repair of aircraft structures, there has been no research on the carbon fibre composite patch repair of steel pressure vessels. Despite many similarities in both of these applications, not all of the results obtained from the patching of aluminum aircraft components can be applied to the patching of damaged pressure vessels. The problem of patching pressure vessels is unique from previous patching investigations because of the following reasons:

(1)   To date, most of the research on patching repairs has been on aluminum panels in aerospace applications. In this investigation, the base material to be repaired (hereafter referred to as the adherend) is a pressure vessel grade steel (ASTM A-516 Gr 70). As a result, the properties of the adhesive that bonds the patch to the steel adherend will have different chemical and mechanical characteristics. The same surface preparation techniques or treatments used in aluminum bonding will lead to different results when applied to steel.

3

Table 1.1, taken from previous experimental work [1.10], shows the relevant mechanical properties of the steel.

Tensile Yield Strength	Tensile Modulus of Elasticity
325 MPa	204 GPa

Table 1.1: Mechanical Properties of ASTM A-516 Gr 70 Steel.

(2)   In this investigation, the patch and the adhesive cure at relatively low temperatures. The advantages of using a low-temperature cure in the repair of structures are numerous. One advantage is that the patch can be easily applied in situ without an external heat source required; this would be difficult to apply in field conditions. The steel adherend simply has to be cleaned using a solvent wipe and a mechanical abrasion process, patched using a two-part epoxy adhesive and composite sheet lay up, and heated minimally using a portable heat source. Another advantage is that lower temperature curing reduces the chance of having residual stresses in the structure. As outlined by Baker [1.1], higher curing temperatures in the bonded assembly of two dissimilar materials has detrimental effects on the strength of the structure. With a higher curing temperature, the different coefficients of thermal expansion between the composite patch and the steel adherend will cause compressive residual stresses in the patch and tensile residual stresses in the adherend after the bonded assembly has cured. Both of these residual stresses have a negative effect on the performance of the patched structure. Note, however, that because the heat for cure is only applied to a local area of the steel adherend, the cooler steel surrounding the patch will limit the degree of thermal expansion.

Low-temperature curing materials have disadvantages as well. Typically, low-temperature curing materials will not perform adequately at higher temperatures. At elevated temperatures, the epoxy resin in both the preimpregnated carbon fibre sheets and in the adhesive layer will soften and cause the material to creep. As well, without vacuum bagging and higher temperature, the cured product is of lower quality. Vacuum bagging reduces the amount of voids in a composite patch and increases its strength. Heat makes the epoxy resin less viscous and this permits better wetting of both the carbon fibre patch and the surface of the steel adherend.

(3)   Unlike the components on an aluminum aircraft, the steel of a pressure vessel to which the patch is to be applied, is relatively thick. This thickness affects both the amount of load that will be transferred to the patch upon loading (a thicker adherend requires a thicker patch) and the pattern by which load is transferred to the patch.

(4)   In a pressure vessel application, the patched structure must be able to retain pressure.

(5)   The patched specimen must be able to withstand a high degree of biaxial loading. Typically, in thin-walled cylindrical pressure vessels, there is a loading ratio of 2:1 in the hoop, σ_h, and axial directions, σ_a, respectively (see Figure 1.1). The fibres in the composite laminate must be aligned so that they are in directions which will resist forces in both directions. Loading in the direction normal to the pressure vessels surface, σ_n, causing the deflection of the material outward, is ignored in this application. Because the patch is relatively thin when compared to the pressure vessel's thickness, the normal stresses in the patch will be minimal. It is assumed also that the constraint

provided by the material surrounding the crack would be sufficient to cause the outward deflections at the crack to be minimal. This last assumption is valid when the crack length, a, is not large when compared to the pressure vessel's thickness, t: $a \sim t$.
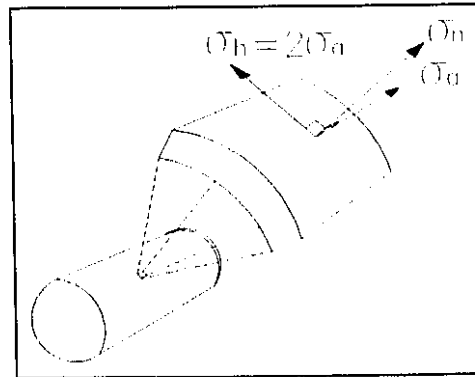
Figure 1.1: Loading in a pressure vessel.

1.4 REDUCING THE GROWTH RATE OF CRACKS

A crack in a loaded structure is one of the most severe forms of damage. In order to safely prolong the life of a structure, the growth rate of the crack must be reduced. In this investigation, the crack growth rate was reduced by both adhering a patch overtop of the crack and drilling holes at the crack's tips.

1.4.1 The Effect of Patching on Crack Growth

The hypothesis that patching will reduce further damage to a cracked pressure vessel is not solely based on previous work done by other investigators. Theoretical foundations for cracking of a predominately linear elastic material indicate that as the load distribution around a crack in a steel structure is altered, the crack driving force is directly affected.

6

The fatigue analysis in this investigation studies the propagation of a long crack under cyclic loading. By experimentally observing how the crack length, a, changes with the number of applied cycles, N, Paris and Erdogan [1.11] described the crack growth rate in a homogeneous material, da/dN, as being a function of the stress intensity factor range, ΔK. Equation 1.1 describes this relationship.

$$da/dN = C(\Delta K)^n \qquad (1.1)$$

C and n are assumed to be material constants[1]. The stress intensity factor range, ΔK, is a function of the amplitude of the cycling far field load, $\Delta\sigma$, the crack length, a, and a geometry factor, $f(g)$, i.e.

$$\Delta K = f(g)\Delta\sigma\sqrt{a} \qquad (1.2)$$

It is also observed that there is a threshold stress intensity factor range, ΔK_{th}, below which the crack does not grow ($da/dN = 0$).

Figure 1.2 shows the relationship between the crack growth rate, da/dN, and the applied ΔK on a log-log scale. The threshold regime in marked by ΔK_{th}. The regime noted by Paris and Erdogan is the linear segment above the threshold regime, ΔK_{th}.

Based on the following two mechanisms, the crack growth rate should be reduced with the addition of a reinforcing patch:

1.   *Reducing ΔK*

     With the support provided by the patch, some of the load applied to the steel

---

[1] C and n are not constant. C and n are interrelated [1.12] and dependent on both the ratio between the minimum and maximum applied loads, R, and the material's loading history. In this analysis, the loading ratio is kept constant at R=0.05 and the loading history for each specimen is kept the same.
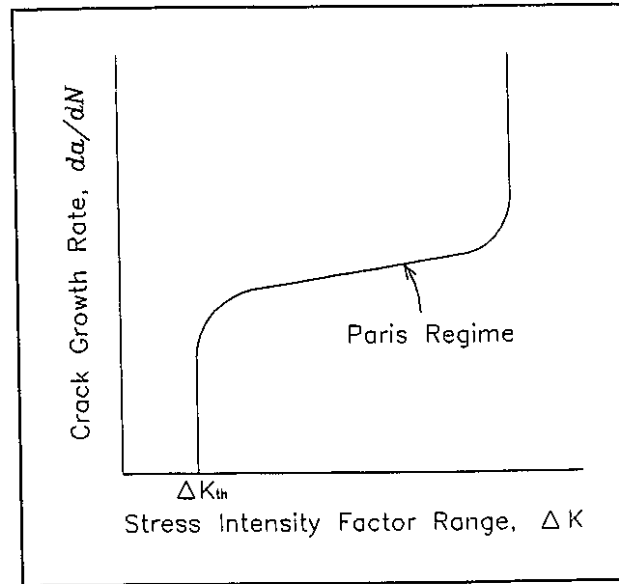
Figure 1.2: The crack growth rate, *da/dN*, as a function
of the stress intensity factor range, ΔK.

structure is transferred away from the steel structure and to the composite patch. This reduction in load to the cracked metal reduces $\Delta\sigma$ which means that the applied stress intensity factor range, ΔK, is reduced as well (equation 1.2). According to equation 1.1, the rate of crack growth should be reduced. In an ideal circumstance, the reduction of load to the cracked structure would completely stop the crack from growing by reducing ΔK below a threshold value, $\Delta K th$, where cracks will not grow.

2.   *Reducing the Crack Opening Displacement*

In a cracked structure under an applied load, the crack opening displacement is a driving parameter in crack propagation. The crack opening displacement under an applied load, however, is partially dependent on the constraint provided by the geometry of the specimen. Bonding a composite patch over the crack provides more constraint; that is, the crack will not be able to open

as much as it would have without a constraining patch. Referring to equations 1.1 and 1.2, the patch has the same effect as decreasing the contribution of the specimen geometry, $f(g)$, as well as $\Delta\sigma$, to crack propagation.

Together, these two mechanisms contribute to an increased resistance to crack propagation in the cracked structure, thereby extending its life.

1.4.2 Reducing the Stress Concentration at the Crack Tip

At the sharp crack tip, there is a large stress concentration when the structure is loaded. Under fatigue loading, this stress concentration can cause a large amount of plastic deformation to accumulate at the crack tip. When the accumulated plastic deformation at the crack tip reaches a certain threshold, the crack will propagate. Thus, damage at the crack tip can be correlated with the plastic deformation. A hole drilled at the tip of the crack reduces the accumulation of plastic damage under cyclic loading by reducing the stress concentration at this point. Based on the above observations, removing the crack tip and using a patch should reduce even further the accumulation of damage to a structure under cyclic loading.

1.5 PROBLEM DEFINITION

The study of the effectiveness of the patched pressure vessel structure can be divided into three inquiries (see Figure 1.3): (1) an analysis of the strength and fatigue resistance of the carbon fibre patch, (2) an analysis of the static strength and durability of the adhesive layer between the composite patch and the steel adherend, and (3) an analysis of the ability of the steel adherend to withstand damage after the application of the patch.
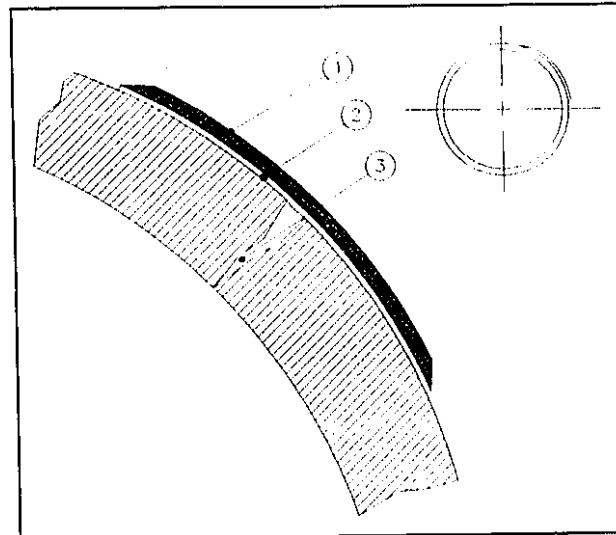
Figure 1.3: A patched pressure vessel showing: (1) the carbon fibre composite patch, (2) the adhesive layer, and (3) the damaged pressure vessel.

1.5.1   Investigating the Composite's Behaviour

The tensile stiffness of the material is important in determining the effectiveness of the patch design. In order to reduce the damage caused by crack initiation and propagation in the steel adherend, the composite patch must be able to: (1) transfer the load away from the cracked structure and, (2) pull the crack closed. To investigate the former, the theory of composite materials is used. The theory of composite materials states that the amount of load supported by each component of the composite structure is dependent on the stiffness of each component and its cross-sectional area. Applying this rule to the patched steel structure indicates that if the composite patch is to carry a large part of the load, then its cross-sectional area and stiffness should be maximized. To investigate the latter, a knowledge of fracture mechanics is required. The degree to which the composite patch will pull the crack closed is dependent on the stiffness of the composite patch.

The ultimate strength of the patch is important as well. Simply, the patch must not fail under an applied tensile or shear loading. Failure of the patch under loading would render the patch useless.

The behaviour of the composite patch is partially a function of its curing cycle. The cure cycle of the composite patch has an effect on the interlaminar shear strength of the epoxy matrix which supports the fibres. This interlaminar shear strength is important in patch design because it determines the ability of the patch to transfer load from one layer of the patch to the next layer of the patch.

The behaviour of the composite patch is also a function of the direction of the fibres. In a pressure vessel application, the composite must be able to withstand biaxial loading. The fibres in the patch must be aligned perpendicular to the crack to retard the crack. For patch durability considerations, however, the patch must also be designed so that it will not crack when loads are applied perpendicular to the direction of the fibres (parallel to the direction of the crack).

1.5.2   Measuring the Effectiveness of the Adhesive Joint

The adhesive layer transfers load, through shear stresses, away from the cracked structure and to the composite patch. In terms of static strength, the effectiveness of the bond is maximized when the shear stresses imposed on the adhesive layer are minimized. The shear stress, however, is dependent on both the compatibility of displacements between the steel adherend and the composite patch and the geometry of the patched structure. The patch should be designed so that the loading between the steel adherend and the composite patch imposes no severe stress gradients in the adhesive layer.

Improving the strength of the bond also means improving the properties of the epoxy

adhesive. Whereas the straining of the structure and the structure's geometry have an effect on the loads imposed upon the adhesive layer, the strength of the adhesive itself is influenced by other factors. In this investigation, different methods of preparing the steel's surface for bonding were investigated; the strength of the adhesive layer is a function of the surface preparation of the steel adherend and the composite patch. Cleaning the surface of any contaminates, exposing a fresh oxide layer for chemical linkages, and mechanical roughening help to provide a stronger and more durable bond.

1.5.3 Investigating the Steel's Response After Patching

As a minimum requirement, a patch should be able to reduce the crack growth rate in a predictable manner so that the life of the pressure vessel can be extended. As a best case condition, the patch would stop a crack in the steel from growing altogether. In general, it is of interest to understand the effect a patch has on the cracked steel's behaviour under an applied cyclic load, an applied biaxial load, and an applied pressure loading environment.

1.5.4 Problem Definition: An Overview

This report investigates each section and presents the results separately. Chapter 2 investigates the material properties of the carbon fibre composite patching material. In chapter 3, the strength of the adhesive layer that joins the two is studied. Chapter 4 investigates the steel's response to applied loads both before and after the patch repair process is employed. Finally, from the data obtained and presented in chapters 2 to 4, some practical rules to pressure vessel repair are outlined in chapter 5.

Table 1.2 outlines the problem that this report investigates.

INVESTIGATING THE COMPOSITE'S BEHAVIOUR

Microstructural Analysis of the Composite Material
Effect of Cure Temperature on Composite Strength
Material Tensile Properties

INVESTIGATING THE EFFECTIVENESS OF THE ADHESIVE JOINT

Effect of the Overlap Length on Bond Strength
Effect of the Surface Preparation Technique on Bond Strength
Effect of the Adherend Thickness on Bond Strength
Effect of Strain Compatibility on Bond Strength

INVESTIGATING THE STEEL'S RESPONSE AFTER PATCHING

Fatigue Crack Propagation in Patched Steel
Fatigue Crack Initiation in Patched Steel
Pressure and Biaxial Loading on the Patched Structure

Table 1.2: Experimental concerns regarding the patching of pressure vessels.

1.6 REFERENCES

[1.1] Baker, A.A., *"Fibre Composite Repair of Cracked Metallic Aircraft Components -Practical and Basic Aspects"*, Composites, Vol. 18, No. 4, September, 1987, pp. 293-308.

[1.2] Ong, C.L., Chu, R.C., Ko, T.C., and Shen, S.B., *"Composite Patch Reinforcement of a Cracked Upper Longeron: Analysis and Specimen Simulation"*, Theoretical and Applied Fracture Mechanics, Vol. 14, 1990, pp. 13-26.

[1.3] Ong, C.L., and Shen, S.B., *"Repair of F-104 Aircraft Nosedome by Composite Patching"*, Theoretical and Applied Fracture Mechanics, Vol. 15, 1991, pp. 75-83.

[1.4] Ong, C.L., and Shen, S., *"Adhesive-Bonded Composite Patching Repair of Cracked Aircraft Structure"*, 34th International SAMPE Symposium, G.A. Zakrzewski, D. Mazemko, S.T. Peters, and C.D. Dean (ed.), 8 May-11 May, 1989, pp. 1067-1078.

[1.5]   Baker, A.A., *"Crack Patching: Experimental Studies, Practical Applications"*, Bonded Repair of Aircraft Structures, A.A. Baker and R. Jones (ed.), Martinus Nijhoff Publishers, 1988, pp. 107-173.

[1.6]   Jones, R. and Callinan, R.J., *"Analysis and Repair of Flaws in Thick Structures"*, Advances in Fracture Research (Fracture 81), Vol. 1, D. Francois (ed.), 5th International Conference on Fracture, 29 March-3 April, 1981, pp. 23-32.

[1.7]   Rose, L.R.F., *"Theoretical Analysis of Crack Patching"*, Bonded Repair of Aircraft Structures, A.A. Baker and R. Jones (ed.), Martinus Nijhoff Publishers, 1988, pp. 77-106.

[1.8]   Alawi, H. and Saleh, I.E., *"Fatigue Crack Growth Retardation by Bonded Patches"*, Engineering Fracture Mechanics, Vol. 42, No. 5, 1992, pp. 861-868.

[1.9]   Yi-Qiang Hu, Pei-Ning Li, Ding-Yi Ju, Hong-Liang Pan, *"Experimental Investigation on a Cracked Body with Adhesive Bonded Reinforcement"*, International Journal of Pressure Vessel and Piping, Vol. 41, 1990, pp. 193-206.

[1.10]   Lefebvre, D. and Ellyin, F., *"Cyclic Response and Inelastic Strain Energy in Low Cycle Fatigue"*, International Journal of Fatigue, Vol. 6, No. 1, January, 1984, pp. 9-15.

[1.11]   Paris, P.C. and Erdogan, F., *"A Critical Analysis of Crack Propagation"*, Journal of Basic Engineering, Transactions of the ASME, Vol. 85, 1963, pp. 528-534.

[1.12]   Kujawski, D. and Ellyin, F., *"A Fatigue Crack Propagation Model"*, Engineering Fracture Mechanics, Vol. 20, No. 5/6, 1984, pp. 695-704.

2.1   INTRODUCTION

The material properties of the carbon fibre composite patch determine the performance of the patched pressure vessel under an applied load. The ultimate strength of the patch must be known so that the patch does not break under an applied static load. The tensile stiffness and the cross-sectional area of the patch must also be known because the deformation of the patched structure under loading and the final geometry of the patched structure are important in determining the efficiency of the patch design. An optimum patch repairs the steel structure to the original stiffness and cross-sectional area of the undamaged steel [2.1]. This study investigates the properties of the composite patch.

The material used for this patching investigation is a room-temperature cure carbon fibre composite. This material was selected over other patching materials for many reasons: (1) the carbon fibres are strong, providing a higher ultimate strength than more conventional glass fibres, (2) the carbon fibres are stiff, with a tensile Modulus of Elasticity along the direction of the fibres similar to that of steel, (3) the laminate is fabricated using a hand lay up procedure, providing a simple and practical approach to repair, (4) the composite is cured at room temperature, eliminating the need for an oven and reducing the amount of residual stresses caused by different thermal expansion coefficients between the composite and the steel, and (5) the patch is fabricated directly on the steel structure.

2.2   THE COMPOSITE'S MICROSTRUCTURE

The preimpregnated composite sheets used in this investigation consist of long unidirectional carbon fibres embedded in a room-temperature cure epoxy. In patching applications with this unique material, the fabrication of the patch begins by applying a two-part epoxy to the steel surface. Next, a carbon fibre preimpregnated sheet is placed

15

(with hand pressure) over top of the epoxy layer. Subsequent layering of the two-part epoxy and carbon fibre preimpregnated sheets is repeated until the carbon fibre patch has been built up to the desired thickness; the purpose of the layering is to allow the two-part epoxy to soften the preimpregnated resin and allow the entire laminate to cure together. The material specification states that the composite will cure in one week at room-temperature. The specification also indicates that shorter curing times occur at higher cure temperatures. Figure 2.1 shows a microscopic view of two layers of the carbon fibre preimpregnated sheet bonded together with a layer of the epoxy resin and cured at room temperature.
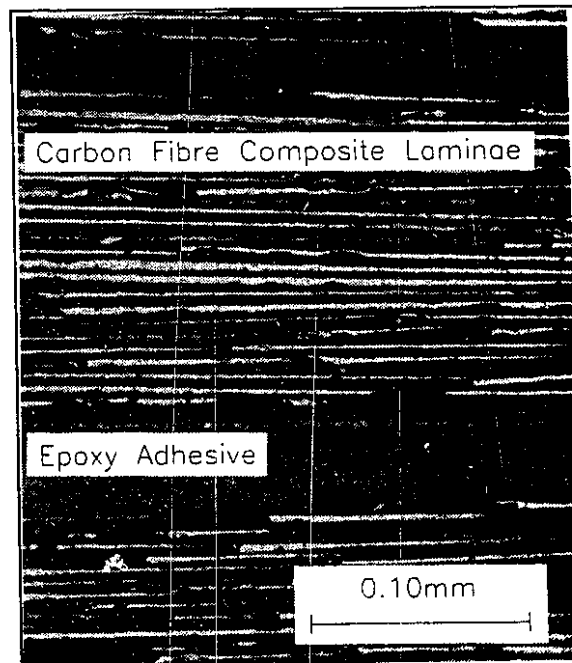
Figure 2.1: A microscopic view of the carbon fibre composite laminate showing alternating layers of carbon fibre reinforced epoxy and unreinforced epoxy.

Two different grades of carbon fibre material were used in this investigation: a material with a lower tensile stiffness (LS) and a material with a higher tensile stiffness (HS).

For the lower stiffness (LS) material, the average thickness[1] of each carbon fibre ply is 0.21mm (8.3x10^{-3}in) (ranging from 0.16mm (6.62x10^{-3}in) to 0.25mm (9.96x10^{-3}in)). For the material with the higher tensile stiffness (HS), the thickness of each carbon fibre ply is 0.14mm (5.5x10^{-3}in) (ranging from 0.10mm (4.17x10^{-3}in) to 0.17mm (6.64x10^{-3}in)). The thicknesses of the epoxy layers between carbon fibre plies, because of the inconsistencies created by the hand lay up procedure, varied largely from 0mm (0in) to 0.10mm (3.80x10-3in), averaging 0.04mm (1.68x10^{-3}mm).

2.3   THE EFFECT OF CURE TEMPERATURE ON PATCH STRENGTH

The microscopic view of the composite illustrates an inherent structural weakness in the carbon fibre patch. Because of the lay up procedure, the laminate has layers of epoxy with no carbon fibre reinforcement. In a patching application, loads are transferred to the patch and between layers of the carbon fibre patch primarily by shear forces. With unreinforced epoxy layers, the shear strength of the composite laminate is reduced. This weak layer within the composite's structure is not as capable of transferring the large shear load as are the reinforced layers.

The cure temperature has an effect on the strength of the epoxy matrix that bonds the fibres together. Initial experimental investigations indicated that the composite assembly has to be cured at temperatures greater than room temperature to get the required shear strength from the composite patch. Generally, elevated temperatures cure the layers of unreinforced epoxy in the composite more fully, producing a stronger bond. Elevated temperatures, however, have disadvantages in patching applications because it is difficult to apply heat to a repaired structure, there are residual compressive stresses created in

---

1   Thicknesses varied within each laminate and between each laminate. The average thickness was determined by measuring the thickness directly under a 10X microscope. The average laminate thickness is the average thickness of samples taken from ten different carbon fibre sheets.

the composite patch after cooling of the bonded assembly, and the steel adherend could change metallurgically upon the application of heat. Optimally, the minimum cure temperature which provides the required strength is desired.

2.3.1   Experimental Specimen Design

Experimental investigation of the effect of cure temperature on the patch strength was done using in-house designed Interlaminar Shear Test Specimens. Because load is transferred from one carbon fibre ply to the next primarily through shear forces, a test specimen was designed to approximate this loading pattern. The test specimen illustrated in Figure 2.2 is the Interlaminar Shear Test Specimen.

Figure 2.2: Interlaminar Shear Test Specimen
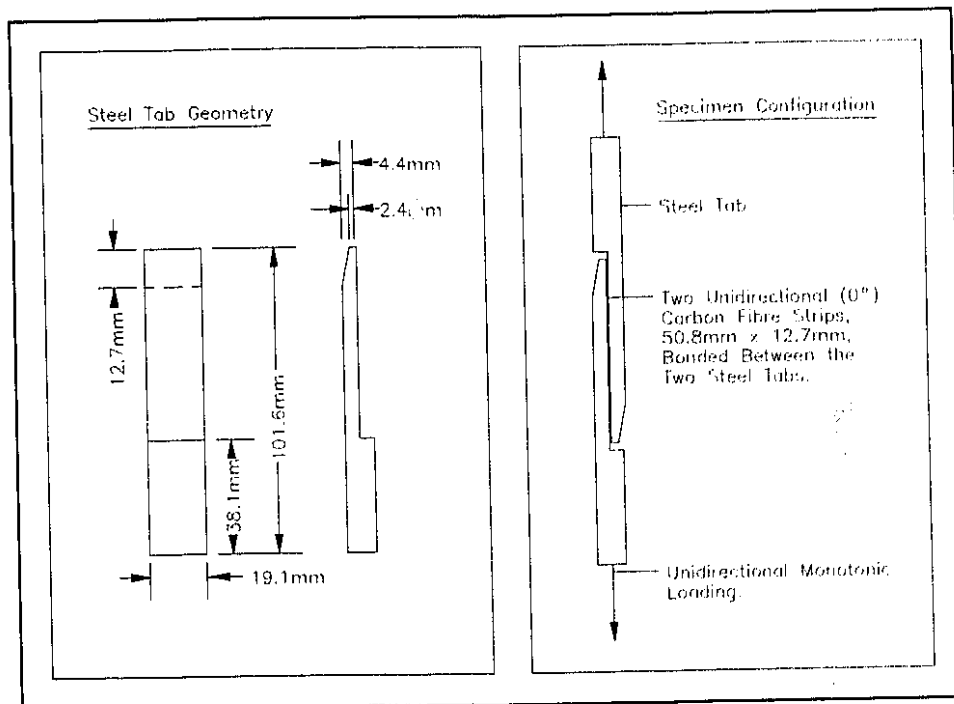
This specimen uses two steel tabs to transfer load from the machine grips to the layers of the composite. The steel tabs are tapered at the end to provide a gradual load transfer

to the composite and sandblasted to provide a good bonding surface. Two layers of composite material, 50.8mm (2.0in) by 12.7mm (0.5in), were then bonded together and to the steel tabs, with their fibre direction running parallel to the direction of the applied load. One specimen was cured at room temperature, 22°C (72°F), for one week. Each of the other specimens was cured for three days at room temperature and then for an additional two hours at temperatures ranging from 38°C (100°F) to 121°C (250°F). The specimen was then pulled in tension under monotonic loading at a constant stroke rate of 1.27mm/min (0.05in/min). The ultimate load applied to the specimens and the failure mode of each specimen was recorded.

2.3.2   Experimental Results

The failure load is defined as the load at which the specimen pulls apart. The failure loads are plotted as a function of the maximum applied curing temperature in Figure 2.3.
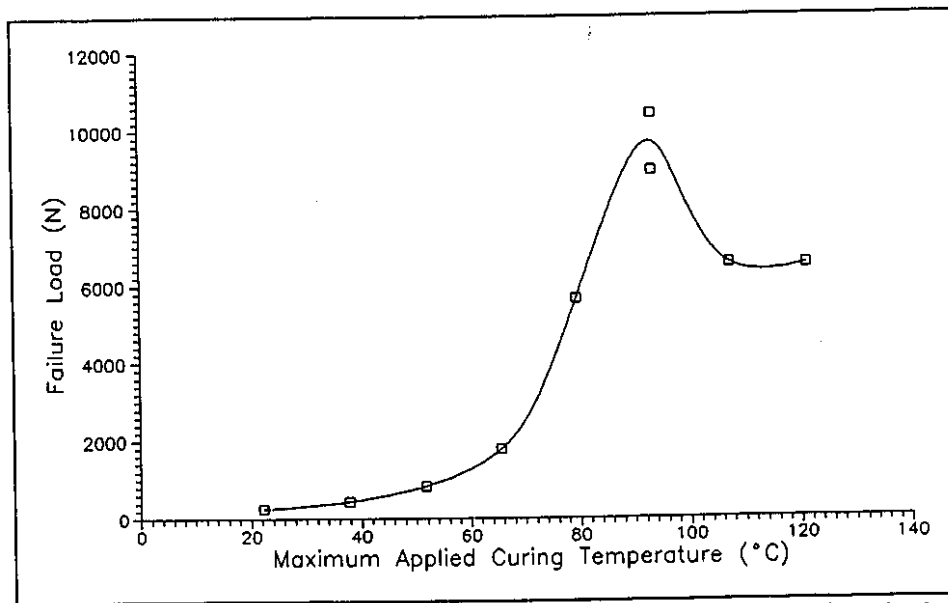
Figure 2.3: The effect of the maximum applied cure temperature on the failure load of the Interlaminar Shear Test Specimen.

Figure 2.3 indicates that of the specimens tested, the strongest composite is obtained when the specimen was cured at 93°C (200°F) for 2 hours. The failure modes of the interlaminar shear specimens were mixed. In some tests, failure occurred between the two layers of carbon fibre preimpregnated sheets, in other tests some failure occurred between the composite fibres in one carbon fibre layer, and in others tests failure occurred in the bond between the carbon fibre sheets and the steel tabs. The failure modes were not observed to be a function of the cure temperature. More probably, the failure mode was a function of the variable epoxy thickness created by the hand lay up technique. Despite this observation, the thickness of the epoxy layers in each specimen was not measured.

2.4 TENSILE STRENGTH AND TENSILE STIFFNESS

1. *Tensile Ultimate Strength:*

The tensile ultimate strength of the patching material must be strong enough to withstand the load applied to it. The ultimate tensile strength is a function of both the material properties of the reinforcing fibres and epoxy matrix, the number of laminate layers, and the direction of the fibres within the laminate layers. Baker [2.2] indicates that the unidirectional patch, with the fibres aligned perpendicular to the direction of the crack, is the most efficient for patch design. In the same reference, Baker also suggests that the unidirectional patch usually has sufficient strain capacity to survive biaxial straining of the metal substrate without splitting. However, in some applications of high biaxial tension, it may be desirable to provide shear and transverse reinforcement by aligning the fibres at $\pm 45°$ and $90°$ to the direction of the applied load. A strong patch, which can withstand biaxial loading, is desired in this pressure vessel patching application.

20

2.   *Tensile Stiffness:*

There are three factors in patch design which are affected by the patching material's tensile Modulus of Elasticity. Firstly, a stiffer patching material will support more of the applied load than a less stiff patching material, causing the load to the cracked steel structure to be reduced. Secondly, a stiffer material is more effective at crack bridging (pulling the crack closed) than a less stiff material. This increased ability to bridge the crack reduces the opening displacement of the crack, and thus, reduces the stress seen at the crack tip of in the steel structure. Thirdly, the stiffness also affects the amount of debonding at the interface between the composite and the steel. Care should be taken not to make the patch too stiff. If the composite patch is too stiff, a large incompatibility of displacements will result at the interface between the stiff composite and the cracked steel specimen, causing large shear stresses in the adhesive. The stiffness of the patch must be chosen so that the efficiency of the load transfer and crack bridging mechanisms are kept to a maximum while the amount of debonding is kept to a minimum.

2.4.1   Experimental Specimen Design

The unidirectional tensile strengths and stiffness of the two different grades of a carbon fibre composite were tested with the loading parallel to the direction of the fibres. In addition, the effect of the fibre direction on tensile strength and Modulus of Elasticity for the lower stiffness (LS) composite material was examined by using specimens with fibres aligned in directions $0°$, $\pm 45°$ and $90°$ to the applied load.

Figure 2.4 illustrates the specimen used to test the composite's ultimate tensile strength and tensile stiffness for the $0°$ fibre direction. The specimen was composed of a 12.7mm (0.5in) width of two 203.2mm (8.0in) layers of composite material. At each end,

21

additional layers, 76.2mm (3.0in) in length, were bonded allowing for a thicker cross-section. Also at each end, 50.8mm (2.0in) tapered aluminum tabs were used. This particular specimen geometry was chosen because it provided a gradual transfer of load from the machine grips to the test area, minimizing any potential stress concentrations at the geometry changes. For the specimens with the $(0°,90°,0°)$ fibre directions, the specimen geometry was similar except that 3 carbon fibre sheets were used in the specimens' test section. For the specimens with the $\pm45°$ and the $90°$ fibre directions, the specimen geometry was similar except that 4 carbon fibre sheets were used in the $\pm45°$ specimens' test section, 6 sheets were used in the $90°$ specimens' test section, and a 25.4mm (1.0in) specimen width was used in both. In order to provide sufficient shear load transfer between the layers of composite material, all of the composite specimens were cured initially at room temperature for 3 days and then at 93°C (200°F) for 2 hours.
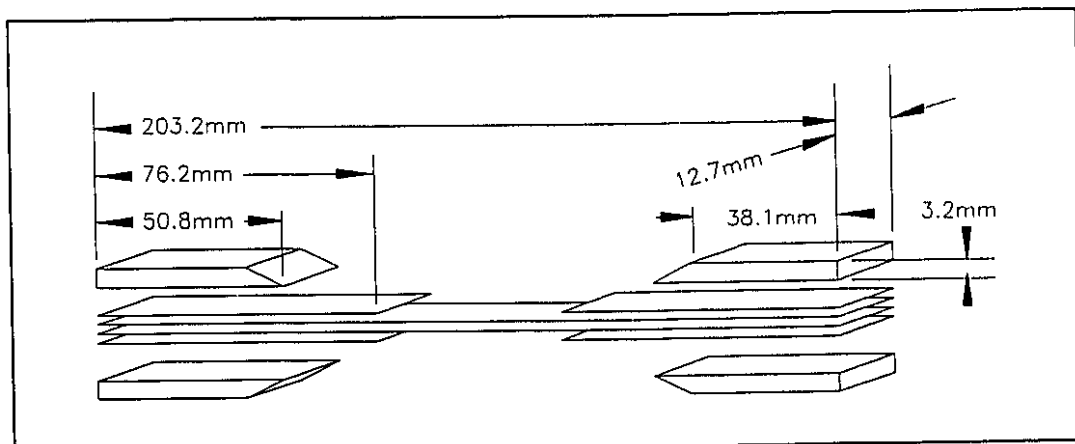
Figure 2.4: The Tensile Test Specimen.

In order to minimize bending, the specimen was loaded in the wedge grips on the testing machine using an alignment block. The ASTM standard on the tensile properties of composites [2.3] recommends the use of two extensiometers to measure the tensile

Modulus of Elasticity, one on each side of the specimen. In the testing of the carbon fibre composite, only a single extensometer (25.4mm (1.0in) gauge length) was used on the wide face of the specimen as the specimen was thin. The potential reduction of strength from induced bending is minimal and thus, was not investigated.

The specimens were monotonically loaded under both a stroke controlled, 1.27mm/min (0.05in/min), or a load controlled, 39 N/min (8.8lb/min), condition. In all cases, the values of the ultimate strength and stiffness could not be correlated to a loading condition. The load values and the strain values were recorded using a computer controlled data acquisition system.

2.4.2 The Longitudinal Tensile Strength of the Composite

The (0°,0°) Lower Stiffness (LS) Tensile Specimen:

In total, 6 lower stiffness (LS) tensile specimens were tested and their results are presented in Table 2.1. The ultimate strength of the specimens is presented in the units kN/m/ply. These units of strength were used because the specimen thickness was highly variable due to the variability of the thickness of the epoxy layers. All 6 specimens had a linear load-strain response. All 6 specimens also displayed brittle failure within the test section with the failure plane being 90° to the direction of the fibres.

Figure 2.5 illustrates the load-strain relationship for one of the tensile specimens. A composite laminate is the strongest and most stiff when loaded parallel to the direction of its fibres. Figure 2.5 illustrates that when loaded along the direction of the fibres, the material's load-strain response is linear. This is consistent with theory which states that when the fibres are aligned parallel to the direction of the load, the fibres are taking all of the load. The non-linear epoxy matrix, in this case, holds the fibres together only.

	Ult. Strength	Ult. Strain	Stiffness
1	283.2 kN/m/ply	1.10%	25,716 kN/m/ply
2	268.4 kN/m/ply	1.12%	23,992 kN/m/ply
3	312.2 kN/m/ply	1.32%	23,739 kN/m/ply
4	335.0 kN/m/ply	1.26%	26,137 kN/m/ply
5	302.1 kN/m/ply	1.16%	25,866 kN/m/ply
6	247.9 kN/m/ply	0.94%	26,388 kN/m/ply
Avg.	**291.5 kN/m/ply**	**1.15%**	**25,306 kN/m/ply**

Table 2.1: The ultimate stresses, ultimate strains, and tensile stiffness of 6 unidirectional (0°,0°) lower stiffness (LS) tensile specimens.
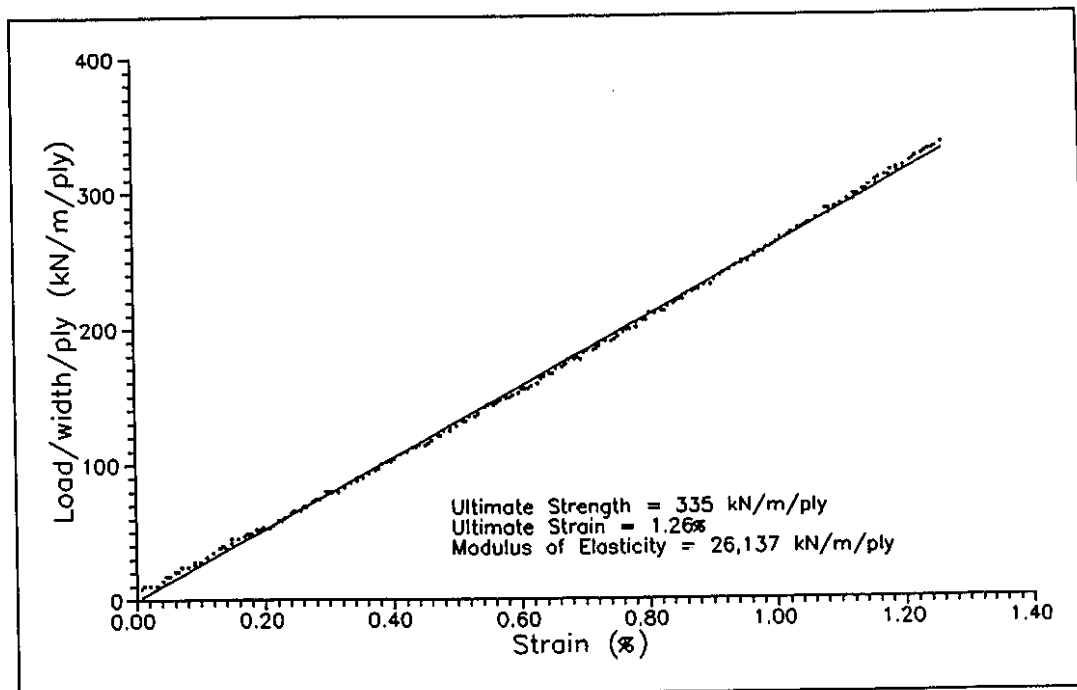
Figure 2.5: The load-strain relationship for a low stiffness (LS) tensile test specimen with loading parallel to the direction of the fibres (0°,0°).

Given that the fibre is taking all of the load, the true stress and modulus of elasticity were calculated. Using microscopic examination, the thickness of each preimpregnated laminae was found to be an average value of 0.21mm. Based on this value and assuming that the thickness of the epoxy layers can be disregarded, the measured range of the

composite material's ultimate stress is between 1150 MPa and 1600 MPa (average of 1390 MPa); the range of the measured modulus of elasticity is between 110 GPa and 125 GPa (average of 120 GPa). These values fall below the suppliers results of 2250 MPa ultimate strength and a stiffness of 144 GPa.

The (0°,90°,0°) Lower Stiffness (LS) Tensile Specimen:

Adding a 90° carbon fibre layer to the already existing 0° carbon fibre layers has certain advantages in this patching application: (1) In a pressure vessel, the principle stresses are aligned parallel to the hoop and the axial directions with a stress ratio of 2:1 respectively. An efficient patch design would align some composite sheets with their fibres aligned parallel to the hoop stresses and some composite sheets with their fibres aligned parallel to the axial stresses. (2) Often, in determining the ultimate tensile strength of the fibres, the 0° tensile specimens tend to exhibit premature splitting of the fibres causing the ultimate strength of the specimen to be reduced. Adding a 90° layer to the specimen prevents this splitting and is more of an indication of the ultimate strength of the fibres. Table 2.2 shows the results for 6 (0°,90°,0°) specimens tested.

	(0°,0°)			(0°,90°,0°)		
	Strength	Strain	Stiffness	Strength	Strain	Stiffness
1	566.4 kN/m	1.10%	51,452 kN/m	711.6 kN/m	1.47%	41,022 kN/m
2	536.8 kN/m	1.12%	47,984 kN/m	666.6 kN/m	1.36%	51,969 kN/m
3	624.4 kN/m	1.32%	47,478 kN/m	692.1 kN/m	1.56%	36,644 kN/m
4	670.0 kN/m	1.26%	42,274 kN/m	722.7 kN/m	1.44%	49,701 kN/m
5	604.2 kN/m	1.16%	51,732 kN/m	633.3 kN/m	1.32%	51,861 kN/m
6	495.8 kN/m	0.94%	52,776 kN/m	685.2 kN/m	1.43%	48,240 kN/m
Avg.	583 kN/m	1.15%	50,600 kN/m	685 kN/m	1.43%	48,250 kN/m

Table 2.2: The ultimate strengths, ultimate strains, and tensile stiffnesses of 6 (0°,90°,0°) and 6 (0°,0°) lower stiffness (LS) tensile specimens.

25

The 90° composite ply prevented the composite from splitting under an applied load and it did not prematurely start to crack itself under the imposed strain produced by the applied load. In addition, in a biaxial loading environment, the 90° composite ply would be able to aid in the load transfer characteristics of the patch, increasing the performance of the patch under biaxial loading. Assuming that the 0° layers take all of the load, the ultimate tensile stress of the fibres is calculated to be between 1510 MPa and 1720 MPa (average of 1630 MPa) and the tensile stiffness is calculated to be between 100 GPa and 124 GPa (averaging 115 GPa). In comparing these values with the (0°,0°) specimens, the average value of the ultimate tensile stress of the fibres went up around 17% where the average value of the tensile stiffness dropped by 4%.

The (0°,0°) Higher Stiffness (HS) Tensile Specimen:

Table 2.3 lists the results for 6 tensile specimens fabricated from the higher stiffness (HS) material. Figure 2.6 shows the load-strain relationship for the higher stiffness (HS) material, plotted on the same scale as Figure 2.5 for comparison purposes.

	Ult. Strength	Ult.Strain	Stiffness
1	98.2 kN/m/ply	0.11%	107,700 kN/m/ply
2	86.5 kN/m/ply	0.25%	35,100 kN/m/ply
3	85.2 kN/m/ply	†	†
4	93.6 kN/m/ply	0.10%	90,300 kN/m/ply
5	109.3 kN/m/ply	0.25%	42,100 kN/m/ply
6	104.1 kN/m/ply	0.16%	62,400 kN/m/ply
Avg	**91.2 kN/m/ply**	**0.17%**	**67,500 kN/m/ply**

†   Strain and stiffness values not available due to slipping of the extensometer.

Table 2.3: The ultimate stresses, ultimate strains, and tensile stiffness of 6 (0°,0°) higher stiffness (HS) tensile specimens.
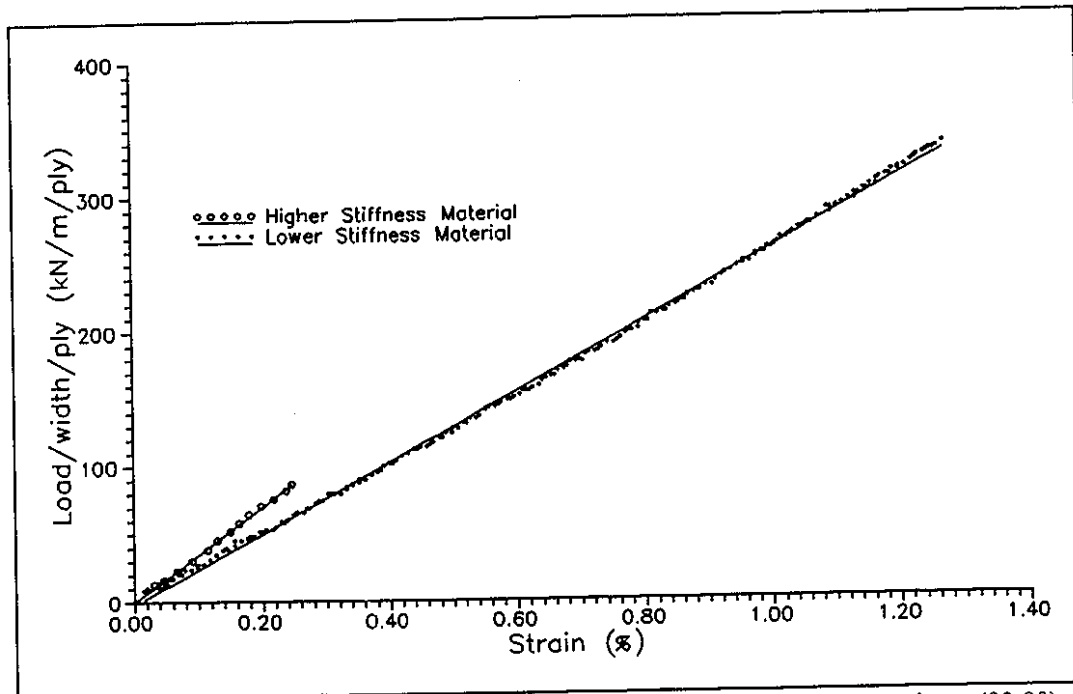
Figure 2.6: The load-strain relationship for a higher stiffness (HS) tensile test specimen (0°,0°).

The higher stiffness (HS) material has a linear load-strain response, like the lower stiffness (LS) material, but has a lower tensile ultimate strength per ply and a lower strain to failure. Despite this, each ply is more stiff than the lower stiffness (LS) material. The experiment confirms the difference in stiffness between the two materials.

It should be noted here that the variations of the stiffness and the ultimate strains for the higher stiffness (HS) material were larger than the variation observed for the lower stiffness (LS) material. These large deviations in results come from a combination of two factors. Firstly, there is an inherent tendency for the composites to display scatter in the results. With current manufacturing techniques, composites contain imperfections (broken fibres, voids, concentrations of unreinforced resin, etc.) which causes different specimens to produce different results. In this application, with the lack of heat and pressure during cure, the imperfections are more profound. Secondly, the cross-sectional

27

areas of the tensile specimens tested were small; only two layers of composite were used in each test area. With a small cross-sectional area, the results for one specimen are highly susceptible to imperfections within the one specimen. As an example, one specimen may contain voids and broken fibres where another specimen may not. A thicker cross section, statistically, tends to be more representative of a larger composite patch. Despite this, all of the higher stiffness (HS) specimens exhibited higher stiffness when compared to the lower stiffness (LS) specimens. Their stiffness were closer to that of steel. Figure 2.7 shows the range of the measured tensile stiffness of the higher stiffness (HS) and lower stiffness (LS) carbon fibre specimens compared to the tensile stiffness of steel.
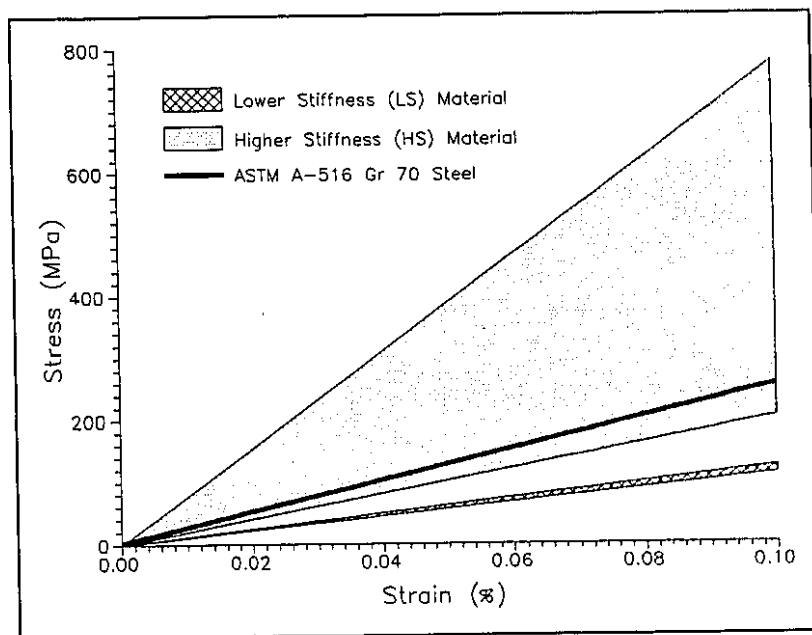
Figure 2.7: A comparison of the stress-strain relationships for the lower stiffness (LS) composite, the higher stiffness (HS) composite, and ASTM A-516 Gr 70 Steel.

2.4.3   The Tensile Strength of the 90° Lay Up Configuration

These tensile specimens were fabricated using 6 layers of the lower stiffness (LS)

28

material with fibres aligned 90° to the direction of the applied load. With this geometry, the epoxy matrix supports the applied tensile load. Table 2.4 shows the results for the 4 specimens and Figure 2.8 illustrates the load-strain response for one of the specimens:

	Ult Strength	Ult Strain
1	4.26 kN/m/ply	0.92%
2	3.71 kN/m/ply	3.01%
3	3.56 kN/m/ply	3.77%
4	5.76 kN/m/ply	1.02%
Avg	**4.32 kN/m/ply**	**2.18%**

Table 2.4: The ultimate stresses of the (90°,90°,90°,90°,90°,90°) lower stiffness (LS) tensile specimens.
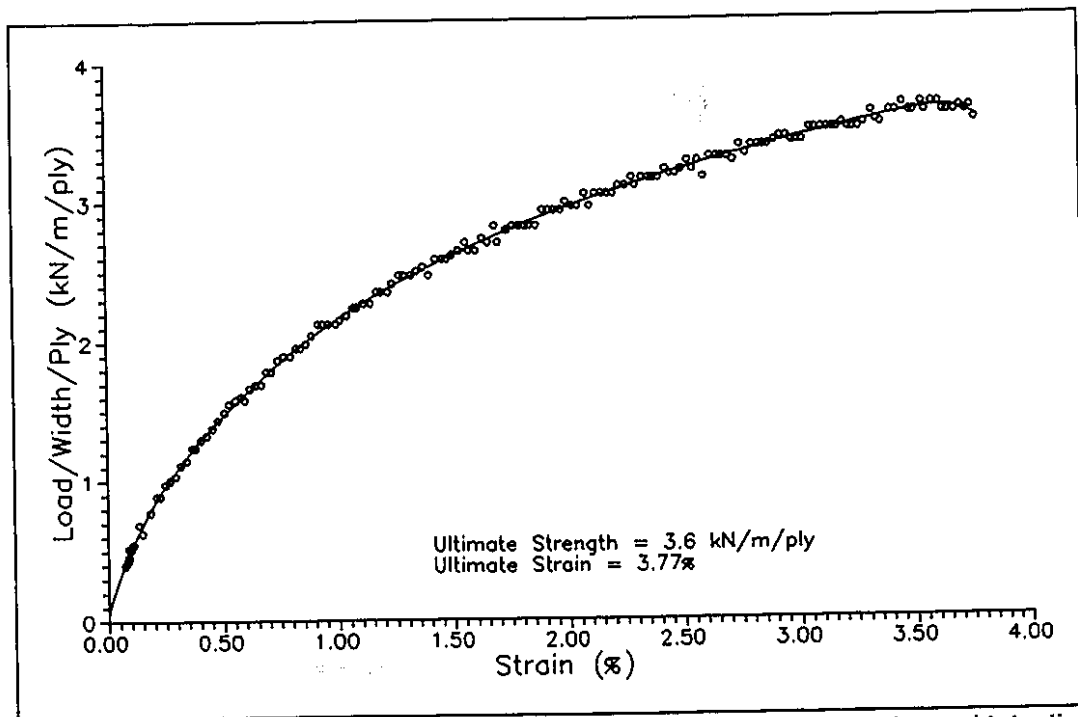
Figure 2.8: The load-strain relationship for a low stiffness (LS) tensile test specimen with loading perpendicular to the direction of the fibres (90°,90°,90°,90°,90°,90°).

The load bearing capabilities of the unidirectional composite patch in the direction $90°$ to the direction of the fibres is both non-linear and weak. When compared to the $0°$ lower stiffness (LS) tensile specimens, the average ultimate load of the $90°$ specimens is only 1.5% of the average ultimate load supported by $0°$ specimens. Despite this, this configuration could withstand on average 17 times more strain until failure. In a biaxial loading application, the unidirectional patch would be able to withstand a certain degree of biaxial straining.

2.4.4   The Interfibre Shear Strength

With fibres aligned in direction $\pm 45°$ to the direction of the applied load, load is transferred through the composite by interlaminar shear stresses. Failure occurs in these specimens by shear along the fibres. Table 2.5 lists the ultimate strengths and strains of each specimen and Figure 2.9 illustrates the load-strain relationship for one specimen.

	Ult Strength	Ult Strain
1	32.6 kN/m/ply	17.6%
2	30.9 kN/m/ply	7.28%
3	30.9 kN/m/ply	15.55%
Avg	**31.4 kN/m/ply**	**13.48%**

Table 2.5:   The ultimate stresses of the $(+45°, -45°, +45°, -45°)$ lower stiffness (LS) tensile specimens.

It is evident that the response of the $\pm 45°$ specimens are nonlinear and weak; the $\pm 45°$ specimens' average ultimate strength being only 10.8% of the average ultimate strength provided when the fibres were aligned parallel to the direction of the applied load. Despite this, the specimens could on average withstand 80 times the imposed strain until failure over that of the $0°$ lower stiffness (LS) tensile specimens.
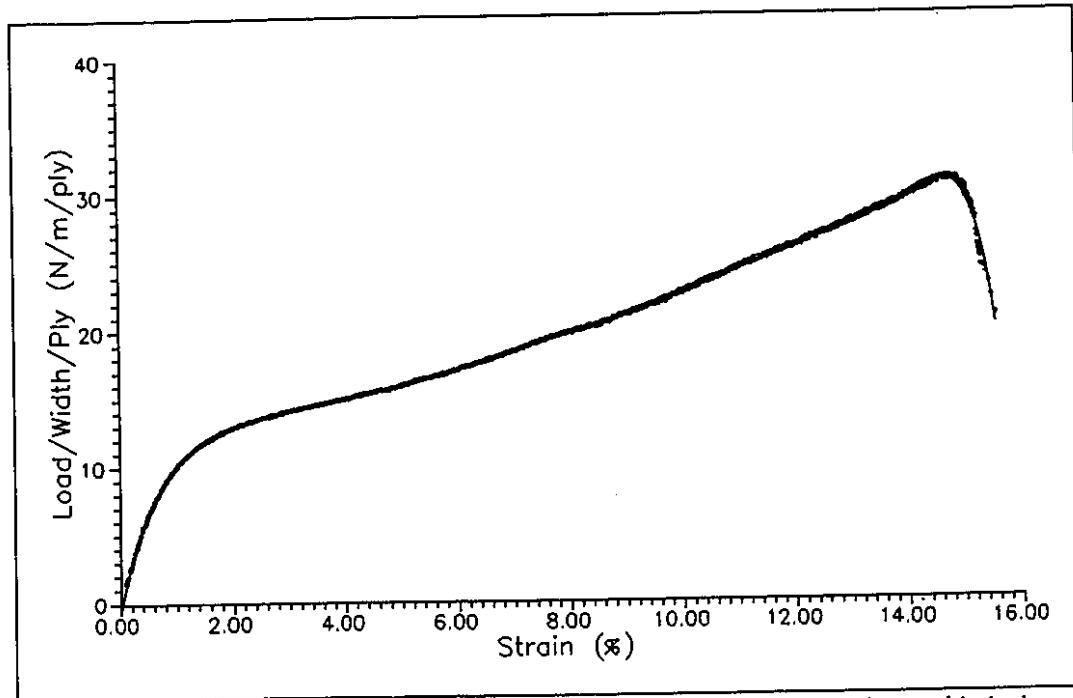
Figure 2.9: The load-strain relationship for a low stiffness (LS) tensile test specimen with the lay up sequence (+45°,-45°,+45°,-45°).

2.5 CONCLUSIONS

The following conclusions summarize the results on the strength and stiffness of the carbon fibre composite patching material:

(1)   In this investigation, the procedure used to fabricate a patch involved the wet lay up of alternating layers of a preimpregnated carbon fibre composite layer and a epoxy adhesive. This lay up procedure produces weak epoxy layers with no carbon fibre reinforcement. These unreinforced epoxy layers are the weakest part of the composite patch when loaded in shear.

(2)   In order to maximize its strength, the carbon fibre patch should be cured at 93°C (200°F). This cure temperature ensures that the epoxy matrix

31

supporting the carbon fibres is strong enough to transfer load, either through tensile or shear forces, from one carbon fibre strand to the next.

(3)   The patch is strong only in the direction of the fibres. Thus, in order for an effective reinforcement to be made, the patch design must align fibres in directions perpendicular to the crack and parallel to the direction of the expected loads.

(4)   The strain to failure of a unidirectional patch is high in directions other than the 0° fibre direction. In a patching application, the fibres of the composite patch are aligned parallel to the direction of the maximum applied load. The patch in directions perpendicular to this applied load will not be able to support any load, but will be able to resist high amounts of imposed strain.

2.6   REFERENCES

[2.1]   Seiner, M.P., *"Stress Field Sensitivity of a Composite Patch Repair as a Result of Varying Patch Thickness"*, Composite Materials: Testing and Design, 10 Vol., ASTM STP 1120, Glenn C. Grimes (ed.), American Society for Testing and Materials, Philadelphia, 1992, pp. 444-464.

[2.2]   Baker, A.A., *"Crack Patching: Experimental Studies, Practical Applications"*, Bonded Repair of Aircraft Structures, A.A. Baker and R. Jones (ed.), Martinus Nijhoff Publishers, 1988, 107-173.

[2.3]   ASTM Designation D3039-93, *"Standard Test Method for Tensile Properties of Polymer Matrix Composite Materials"*.

3.1 INTRODUCTION

In a patching process, the structural durability and effectiveness of the patch depends largely on the properties of the adhesive which joins the two materials together. The adhesive layer between the steel adherend and the composite patch must be able to transfer a cyclic shear load to the patch, for a given number of cycles, while resisting forces such as peel stresses, stress concentrations caused by edge effects, imperfections caused by unclean bonding conditions or a corrosive environment, and local delamination between the adherends. In order to obtain an optimal patch design, the strength of the adhesive layer must be optimized for the adhesive-adherend structural configuration.

This analysis investigates the strength of the adhesive layer between the carbon fibre composite patch and ASTM A-516 Gr 70 steel.

3.2 STATIC STRENGTH OF THE BOND

3.2.1 Loading in the Adhesive Layer

A patched structure consists of three structural components: (1) a parent or base material to which the patch is to be adhered to, (2) a patch, and (3) an adhesive layer which joins the two.

In the patched structure, load is transferred away from the damaged adherend to the patch by way of shear load transfer through the adhesive layer. For this reason, the shear strength of the adhesive layer should be maximized in order to provide the strongest patch design; the stronger the adhesive bond, the stronger the patch can be designed so that more load can be transferred away from the cracked structure. Peeling stresses in the adhesive layer (at the edges of the patch) also affect the strength of the

33

bond. The peeling stresses are minimized with the use of a tapered patch.

Currently, there is no universally accepted failure criteria for adhesive bonds [3.1]. Ideally, Hart-Smith [3.2] stated that the adhesive layer should be the strongest component of the bonded assembly and should exceed the strengths of the other components by at least 50%. The reasoning, based on fracture mechanics, is that any delamination or defect in the adhesive layer behaves very similarly to a crack in a constrained structure. If the surrounding adherents are constrained and strong, a small delamination in a weak adhesive layer will tend to zip through the entire material when loaded in shear. Linear elastic fracture mechanics is not a good model for predicting failure in the adhesive layer because the analysis is localized to analysis of the crack tip. Most predictions of adhesive strengths come from experimental examination or finite element modelling of the materials used for a particular bond.

In designing the patch it is important that the adhesive layer is able to remain bonded during the fatigue life and at no point, fail in shear. Complete failure of the adhesion between the steel and the composite patch would render the patch ineffective. The adhesive layer should also be over designed in order to account for possible delamination due to local imperfections and impurities in the bond.

3.2.2 Shear Stress Distribution

Bonded joint theory states that the shear stress distribution in the adhesive layer between a parent material and an applied patch is not uniform throughout the length of the patch. Figure 3.1 illustrates, schematically, how the shear stresses are distributed between two materials in shear loading. The maximum shear stresses are located in the adhesive layer at the ends of the bond where displacement differences, due to geometry changes and a loading gradient between the patch and the adherend, are the largest. The shear stresses

at the centre of the bond, where the displacements of the adherend and the patch are compatible, are minimal, uniform, and elastic.
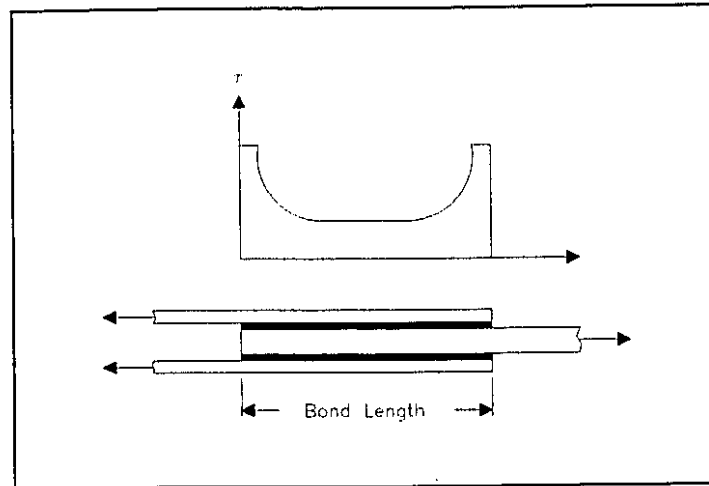
Figure 3.1: The shear stress distribution in the adhesive layer.

3.2.3 Factors Affecting the Shear Strength of the Adhesive Layer

For any particular adhesive-adherend combination, the shear stress distribution is dependent on a number of factors. The following four factors affect the mechanical behaviour of the bonded structure and have been considered in this investigation: (1) the overlapping length of the patch on the steel on either side of the discontinuity, (2) the surface preparation of both the adherend and the patch, (3) the compatibility of strain between the adherend and the patch, and (4) the adherend thickness. Other factors also contribute to the shear strength. Chemical cohesion forces and the quality of the oxide formed on the adherend surface, adhesive thickness, environment, adhesive layer shear modulus, and adherend modulus are also influencing factors but they are not considered here. In order to minimize the experimental scatter in this investigation, however, these factors were kept constant throughout the investigation.

Bond Overlap:

The bond length is a critical parameter in the bond durability affecting both the shear strength properties of the structure and its resistance to local delamination. Figure 3.2, illustrates the effect of overlap length on the shear stress distribution in the adhesive layer. For a short bond overlap length, the adhesive layer between the patch and the adherend is loaded to a fully plastic condition under an applied load. For a longer bond overlap length, under the same applied load, the shear load is applied to a larger bond area. As a result, the stresses in the centre of the bonded area are reduced (because of the reduced incompatibility of displacement between the steel adherend and the patch at the centre of the bond) creating an area where the adhesive is loaded elastically; plastic shear stresses are concentrated at the ends of the bond area. As the length of the overlap is increased further, the elastic regime between the plastic shear stresses at either end of the bond becomes longer. An over-designed bond, in terms of bond overlap length, has advantages. For example, any delamination in the adhesive layer would have minimal effect on its ultimate shear strength. A delamination would only cause a reduction in the elastic region of the bond which carries a minimal amount of the load. Also, the large elastic trough in the shear stress distribution would ensure that there is minimal creeping of the bond under sustained static loading.

With the use of a carbon fibre composite patch on a cracked steel specimen, the assumption is that there will be local delamination of the composite patch from the loaded steel structure as a result of the large displacement incompatibilities at the crack tip. If the patch length is long enough, it is assumed that the structure will act similar to a bonded structure with a large overlap and a debonded region in the centre of the overlap area. In general, it is assumed that the delamination around the crack tip will have little effect on the shear strength of the adhesive bond.

Figure 3.2: The shear stress distribution in the adhesive layer for different bond overlap lengths. Figure taken from [3.2].

Surface Preparation of the Steel Adherend and the Composite Patch:

The surface preparation of the steel adherend affects the strength of the adhesive layer. Minford [3.3] states that there are both chemical and mechanical contributions to the adhesion between adhesive and adherend. Part of the bonding strength comes through intermolecular bonding. In metals, the ability of the surface to bond in this manner is largely dependent on the oxide layer formed on the surface [3.4]. Removal of an old contaminated surface creates a fresh oxide layer which is sufficient to prepare the surface for bonding. Another portion of the strength come from mechanical linking of two roughened surfaces. Roughing or abrading the surface will provide interlocking geometries which will improve the adhesive layer's resistance to shear. For steel, sources [3.5] indicate that surface abrasion is all that is required to prepare the surface for both chemical and mechanical bonding. Mahoney [3.4], suggests that if an abrasion process is not possible, then the steel adherend should be soaked in a concentrated HCl bath for 3-10 minutes and then rinsed with distilled water.

37

Chapter 3: The Adhesive Bond

For the composite patch, the need for surface preparation is avoided by co-curing the patch with the adhesive bond [3.5].

Displacement Compatibility Between the Steel and the Composite Patch:

The tensile stiffness of the composite patch has an effect on the performance of the patched structure under loading. Consider a fully bonded double lap shear specimen (shown in Figure 3.3) loaded in the linear range of the stress-strain curve for the adhesive.
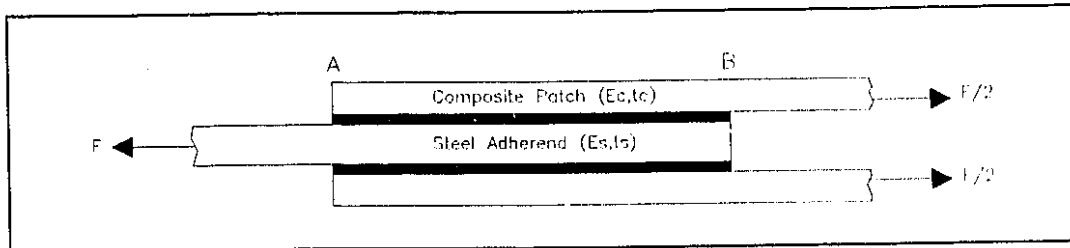
Figure 3.3: A fully bonded Double Lap Shear Specimen.

As previously explained, the shear stresses in the adhesive layer between the steel and the composite patch are not uniform throughout the length of the bond; the stress gradients are the highest at points A and B (see Figure 3.3). At point A, the steel is strained by the applied load and the composite material is not strained at all; this creates an incompatibility in the displacements of the two adherends, and thus a stress concentration, at this point in the adhesive layer. At point B, the composite is strained by the applied load and the steel is not strained at all creating another stress concentration at this point in the adhesive layer. At point B, the strain in the composite for a double lap shear specimen is proportional to the applied load, F, the tensile stiffness of the composite, E_c, the thickness of the composite layer, t_c, and the width of the patch, w:

$$\varepsilon_c \sim \frac{F}{2 E_c t_c w} \qquad\qquad (3.1)$$

Equation 3.1 illustrates that as the stiffness of the composite layer, E_c, increases and all other variables are kept constant, the maximum strain at this point will be reduced and tend towards the strain in the steel adherend. This reduction in strain reduces the incompatibility of displacements between the composite and the steel at this point; reducing the stress concentration.

Reducing the stress concentration at point B, however, only means that there will be an increase in the stress gradient at point A. Figure 3.4 illustrates that as the maximum stress is reduced at point B, the portion of the adhesive around point B which is yielding decreases. At the same time, because this load must eventually be transferred to the composite, the portion of the adhesive around point A which is yielding increases. John, in his investigation on composite joints, noted that *"when a critical portion of the adhesive in a bonded double-lab joint exceeds or equals its shear yield stress, the joint is deemed to fail"* [3.1,p57]. Thus, an increase of bond strength between the steel and the composite can be obtained when the product of the stiffness and the total thickness of the composite patch (the total thickness being the sum of the thicknesses on each side of the double lap shear specimen), $E_c t_c$, tends towards the product of the stiffness and the thickness of the steel layer, $E_s t_s$.

$$E_c t_c \rightarrow E_s t_s \qquad\qquad (3.2)$$

This equalizes the amounts of yielding at points A and B in the adhesive layer.
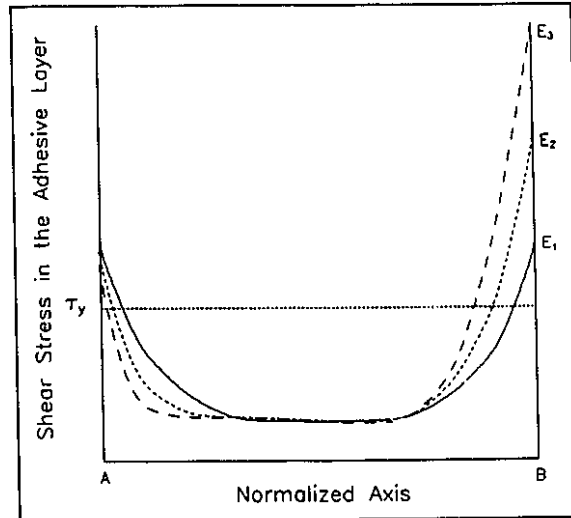
Figure 3.4: The shear stress distribution in the adhesive layer as a function of the stiffness of the composite patch: $E_1 > E_2 > E_3$.

The Adherend Thickness:

The thickness of the steel adherend layer also has an effect on the strength of the adhesive bond. From the previous section, it was determined that increased strength in the adhesive layer between the steel and the composite can be obtained when the product of the stiffness and the thickness of the patch, $E_c t_c$, tends towards the tensile product of the stiffness, E_s, and the thickness, t_s, of the steel layer (see equation 3.2). Thus, keeping the material properties of the steel and the patch constant, and keeping the thickness of the composite patch constant, a change in the thickness of the steel adherend would result in a change in the bond strength.

3.3 DURABILITY OF THE BOND

This investigation does not include an analysis of the durability of the adhesive bond. Durability under constant amplitude fatigue loading is discussed in chapter 4.

3.4   EXPERIMENTAL INVESTIGATIONS

In order to get preliminary results for the bond strength of the patched steel structure, standard Double Lap Shear Specimens were tested [3.6]. Factors such the bond overlap length between the carbon fibre and the steel adherend, the surface preparation of the steel adherend, the adherend thickness, and different patching materials were studied. The tests here were conducted to give an idea of trends, rather than precise values, and to aid in the understanding of the patching process.

3.4.1   The Double Lap Shear Specimen

The examination of the shear strength of the adhesive layer between the steel specimen and the carbon fibre composite patch was done using a Double Lap Shear specimen. This specimen was employed because it provided a simple method of determining the bond characteristics without introducing bending stresses into the adhesive bond while minimizing the peel stresses at the end of the composite patch. Figure 3.5 shows the dimensions of the Double Lap Shear Specimens. The two steel tabs were bonded together using three layers of unidirectional carbon fibre composite material bonded on each side. The ends of the carbon fibre patch were tapered to minimize stress concentrations at these locations and to reduce the amount of peel stresses induced by a changing material geometry.

3.4.2   Test Results

The experimental values that are of interest are: (1) the maximum strength generated by the bond, (2) the overlap length necessary to generate this strength, and (3) the mode of failure of the bond. The following sections detail the results of the investigations on overlap length, surface preparation technique, patch stiffness, and adherend thickness.
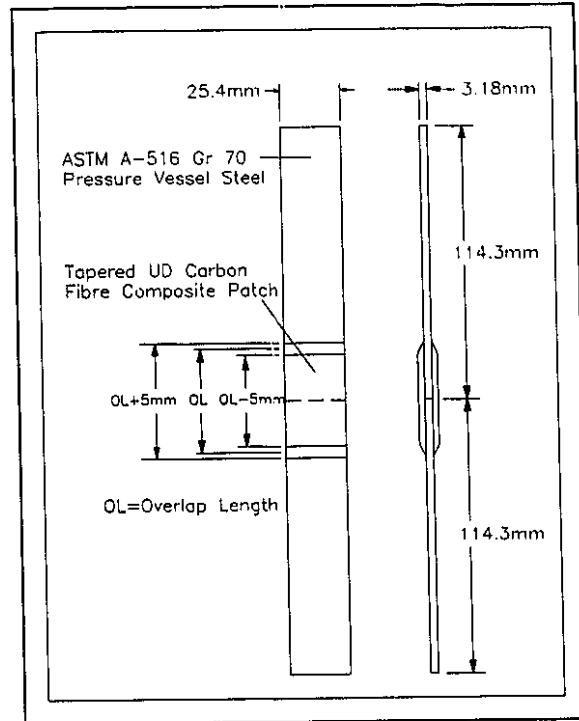
Figure 3.5: The Double Lap Shear Specimen

Overlap Length:

The overlap length was varied in the specimen to determine the minimum overlap length which would provide the maximum adhesive shear strength. In this investigation, the overlap length refers to the average length of the carbon fibre laminae in the patch.

The steel tabs were prepared using a surface preparation technique of: (1) degreasing the steel specimens with an acetone wipe, (2) hand grinding the steel specimens with 80 grit sandpaper, and (3) cleaning the specimen with an acetone wipe. After letting the prepared surface sit for a minimum of 1/2 hour, the composite patch was applied and the assembly was then left to cure for three days at room temperature, 22°C (72°F), and then cured in an oven for 2 hours at 93°C (200°F).

During testing, the specimens were clamped into a tensile testing machine with self-aligning clamps to ensure axisymmetric loading and loaded with a constant stroke rate of 1.27mm/min (0.05in/min). The load at failure plotted (Figure 3.6). As the overlap length of the bonded patch is increased, so is its ultimate strength. This trend continues until the overlap length is approximately 65mm (2.55in), where the ultimate shear strength of the bonded assembly, around 780 kN/m (4455lb/in), is insensitive to overlap length. The line in Figure 3.6 shows the trend of the experimental results.
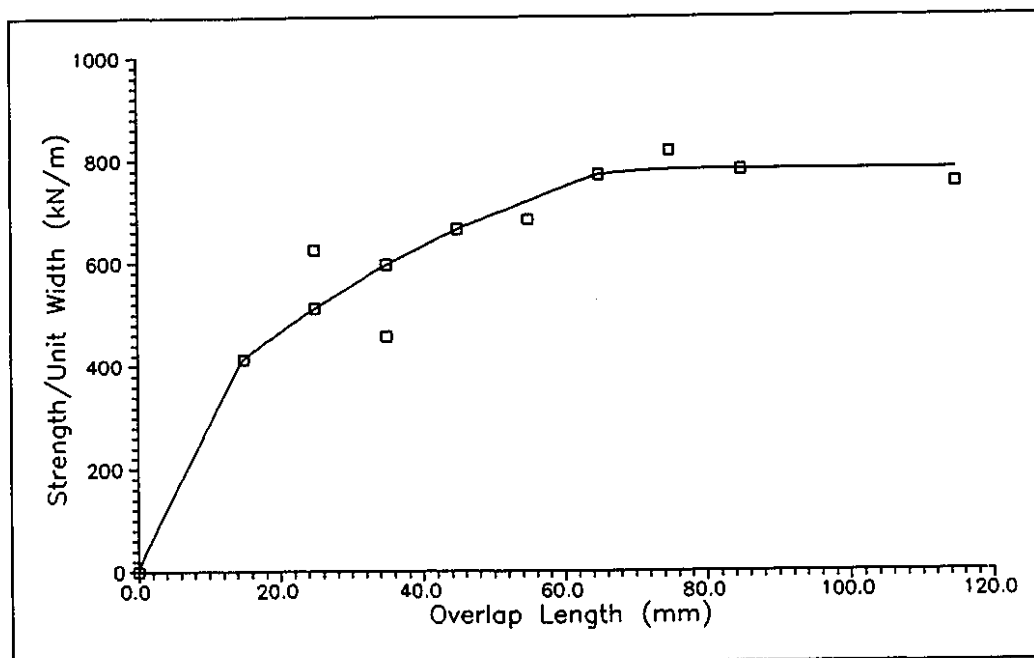
Figure 3.6: The influence of overlap on the maximum and minimum adhesive shear strengths in bonded joints: experimental results.

When the overlap length was small (under 65mm (2.55in)), failure occurred in the adhesive layer only, indicating that the adhesive layer was the weakest component of the assembly. As the bond overlap length increased from the overlap length sensitive regime (under 65mm (2.55in)) to the insensitive regime (over 65mm (2.55in)), failure started to occur in the carbon fibre patch. Fibre breakage at the ends of the carbon fibre laminate in the laminae closest to the bonded steel indicates that the bond is becoming stronger

than the carbon fibre patch. Similar failure modes were observed by John [3.1] who stated that as the overlap length was increased, the mode of joint failure changed from cohesive failure in the adhesive to interlaminar failure in the composite substrate.

These experimental results are consistent with those published in the Engineering Materials Handbook [3.2]. Figure 3.7 illustrates that the static strength of the bonded joint is quite insensitive to long overlap. With sufficiently long overlap length, the majority of the bond stresses are concentrated at the ends of the patch where the bond stresses at the middle of the patch are minimal. Increasing the overlap length would not alter the critical stresses at the ends of the bond. Also, as the overlap length gets larger, and the bond becomes stronger, failure occurs in the composite patch.
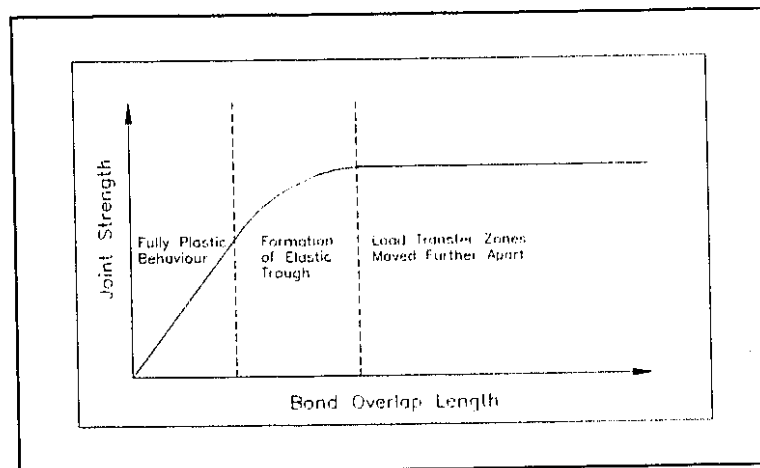
Figure 3.7: The theoretical influence of overlap on the adhesive shear strengths in bonded joints. Figure adapted from [3.2].

Surface Preparation Technique:

Three different surface preparation techniques were employed to the steel adhered:

1.   Surface Abrasion (Hand Grinding):

        The steel surface was first wiped with acetone. The surface was then

roughened with 80 grit sandpaper and cleaned again with acetone. The exposed surface was allowed to sit for 24 hours.

2.   Surface Erosion (Sandblasting):

The steel surface was sandblasted and then allowed to sit for 24 hours.

3.   Chemical Treatment:

The steel was degreased by wiping with tetrachloroethylene. The specimens were placed in a HCl bath (1pt/wt HCl;1pt/wt distilled water) for 10 minutes. The specimens were dried in the oven for 10 minutes at 77°C (170°F).

Following the surface preparation procedure, the specimen was initially cured at room temperature for three days and then at 93°C (200°F) for 2 hours. After cure, the specimens were pulled at a rate of 1.27mm/min (0.05in/min) until failure. Figure 3.8 shows the test results comparing the three surface preparation techniques.
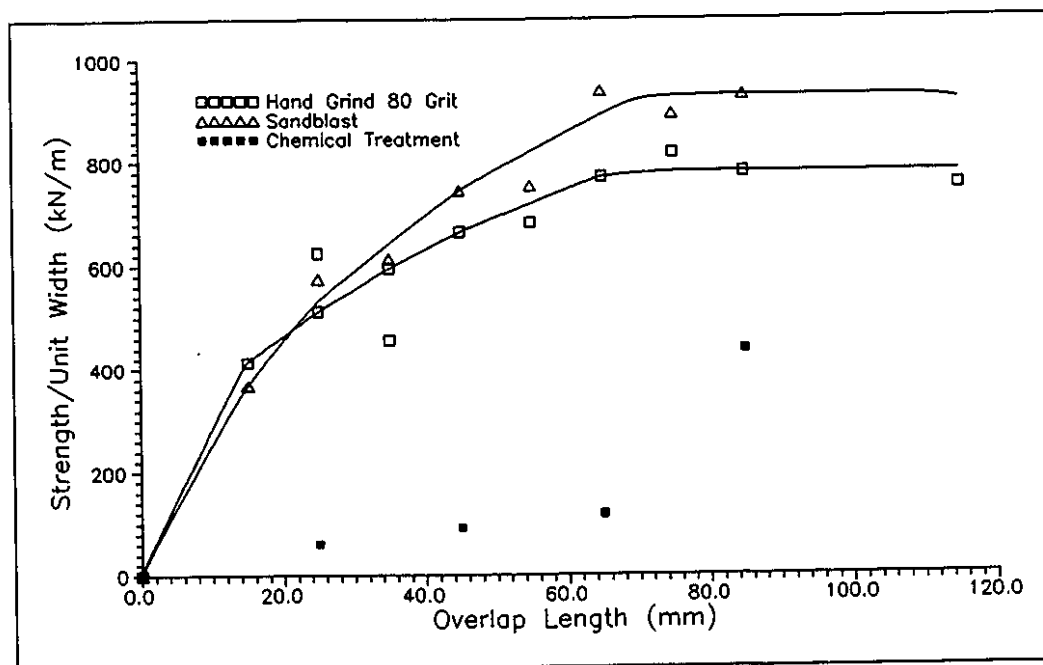
Figure 3.8: The effect of the surface preparation technique on the maximum strength and minimum required bond overlap length in bonded joints.

It is evident that surface erosion technique (sandblasting) provides the best adhesive bond strength with an upper tensile strength of 920 kN/m (5250lb/in); an 18% increase in the ultimate strength of the specimens prepared using the surface abrasion technique. The chemical treatment produced results that were unpredictable and low. It appeared that the dried HCl residue on the surface of the steel has a negative effect bond strength. Baker [3.5] suggests that chemical treatments should be avoided because it is difficult to apply a chemical process in field conditions and because it is possible to entrap chemicals in the bond; encouraging corrosion of the metal substrate. This study confirms that chemical treatments do not result in good bond strength.

The surface preparation technique did not have an effect on the minimum bond overlap length required for maximum bond strength. For both the surface abrasion and the surface erosion technique, the minimum required overlap length was close to 65mm (2.55in). This result is consistent with theory. In each of the three specimens tested, the stress distribution along the adhesive layer was the same because the same specimen geometry and the same materials were used in each. As a result, the minimum required overlap lengths for maximum bond strengths would be the same in each. The difference between the specimens lie in the maximum obtainable strength. Improving the mechanical and chemical linking means that more load can be supported by the bond, despite the loading distribution. In other words, the minimum overlap length required is a function of the material properties and geometry of the composite patch and the steel adherend. The maximum obtainable strength is a function of the quality of the chemical and mechanical linkages that bonds the two. Improving the surface preparation technique essentially increases the bonding potential between the two adherends; amplifying the strength of the adhesive layer.

Displacement Compatibility Between the Steel and the Composite Patch:

In order to test the effect of the compatibility of the adherend displacements on the ultimate shear strength and overlap length required, a different patching material was applied to the double lap shear specimens. For the purpose of comparison, a higher stiffness (HS) composite material is compared to the lower stiffness (LS) material tested earlier. Both specimens utilized the mechanical erosion (sandblasting) surface preparation technique, and both specimens were cured initially at room temperature (22°C (72°F)) for three days and then in the oven for 2 hours at 93°C (200°F).

The same geometry employed in the investigations of bond overlap and surface preparation was employed except that the number of layers on each side of the patch was increased to 12. More layers were required because the thickness of the higher stiffness (HS) composite laminate is smaller (see section 2.2), making the strength per ply smaller as well. The increased thickness was necessary to ensure that the specimen would fail in the adhesive layer between the patch and the adherend, not by tensile failure in the composite patch alone.

Figure 3.9 shows the results for the ultimate load as a function of overlap length for the lower stiffness (LS) and the higher stiffness (HS) materials. Figure 3.9 illustrates that using a different composite material has different effects on both the ultimate strength of the lap shear specimen and the overlap length required to obtain this maximum thickness. The maximum load obtained using the higher stiffness (HS) material is 1030 kN/m (5900lb/in) and this occurred at an overlap length of around 50mm (2.0in). This maximum load is a 12% increase over the maximum load which could be obtained using the lower stiffness (LS) material.

The results illustrate two important points. Initially, using a composite material with a

stiffness more similar to that of steel increases the strength of the bond. By examining the stresses in the adhesive layer, it becomes evident that the amount of shear stress concentrated at the end of the bond is reduced. Secondly, the minimum bond overlap length necessary for the strongest bond is reduced. With a stiffer material, the amount of strain in the both the patch and in the steel adherend, under an applied load, would be similar. This compatibility in the strain would produce less straining in the adhesive layer; thus a smaller bond length is required to generate strength. These results are consistent with Siener [3.7] who indicates that as the joint efficiency improves, the overlap length required for maximized joint strength is reduced. These results are also consistent with equation 3.2. Using a stiffer patch with a thicker cross sectional area makes the product, $E_c t_c$, approach the product, $E_s t_s$. The bond then becomes stronger.
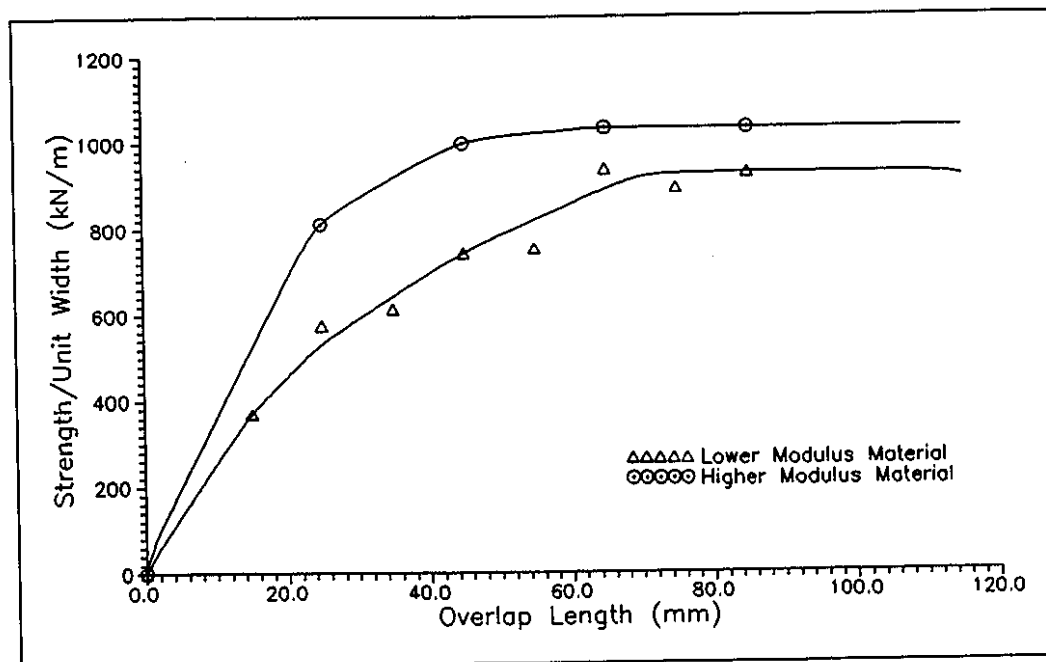
Figure 3.9: The effect of patch stiffness on the maximum strength and the minimum required overlap length in bonded joints.

Adherend Thickness:

In order to test the effect of the adherend thickness on the ultimate shear strength and the minimum overlap length required, the thickness of the adherend was increased from the 3.2mm (⅛in) to 15.9mm (⅝in). These shear specimens were prepared using a mechanical erosion (sandblasting) surface preparation technique. Three layers of lower stiffness (LS) carbon fibre composite were placed on each side of the specimen. The results were compared with the thin adherend shear specimens prepared in a similar manner.

Figure 3.10 shows the results of the specimens tested.
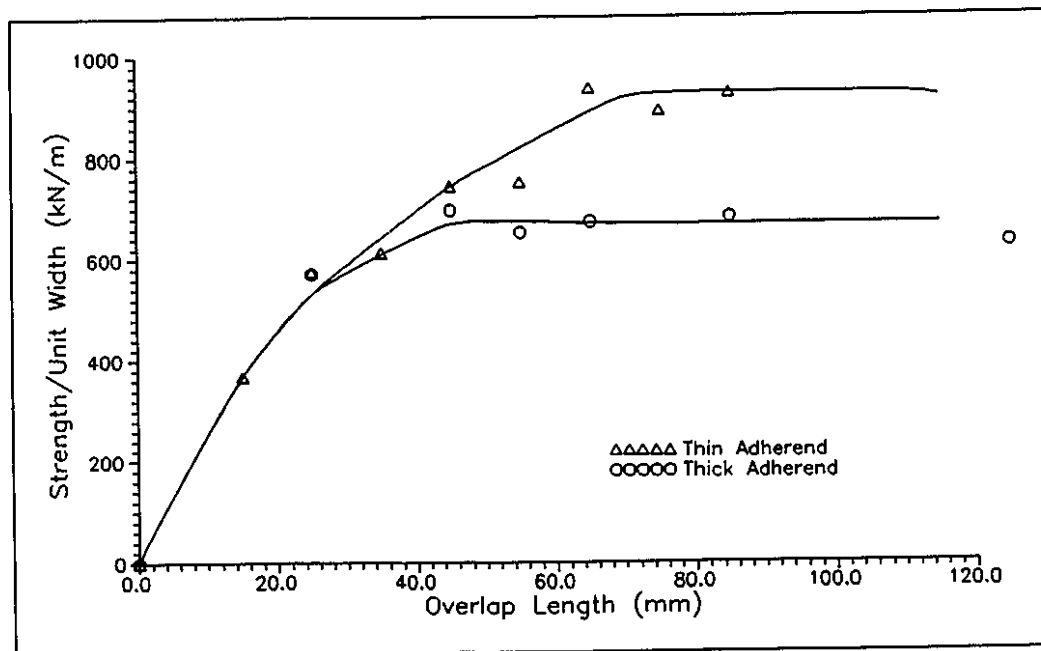
Figure 3.10: The effect of adherend thickness on the maximum strength and the minimum required overlap length in bonded joints.

From Figure 3.10, it is evident that a thicker steel adherend reduces the maximum obtainable strength of the double lap shear specimen to 670 kN/m (3830lb/in). Equation

49

3.2 stated bond strength would be increased if the product of the stiffness and the total thickness of the composite patch, $E_c t_c$, approaches the tensile product of the stiffness and the thickness of the steel layer, $E_s t_s$. For the thin steel adherend, plotted in Figure 3.10, both the tensile stiffness of the composite patch and the total thickness of the composite patch are smaller than those of the steel specimen. Thus, increasing the thickness of the steel adherend only decreases the bond strength.

For lower overlap lengths, when the straining in the bond creates a plastic or near-plastic response in the adhesive, the effect of the adhesive thickness on bond performance diminishes. This effect is seen in Figure 3.10 where the bond strength becomes similar at overlap lengths of less that 25.4mm (1.0in).

3.5   CONCLUSIONS

The following conclusions are drawn from the results of the experimental investigations on the standard Double Lap Shear specimens. All of the specimens were prepared by joining ASTM A-516 Gr 70 pressure vessel steel to either a lower stiffness (LS) or a higher stiffness (HS) carbon fibre composite material.

1.   There is a minimum length of overlap required to maximize the strength of the adhesive bond in a lap joint configuration. For a double lap shear specimen, using a lower stiffness (LS) carbon fibre composite patch and prepared using a sandblasting technique, the minimum overlap required is 65mm (2.55in).

2.   The surface preparation technique of the steel affects the maximum strength of the bond but not the minimum overlap length required for maximum strength. The surface erosion technique (sandblasting) provided a better surface for bonding over that of the hand abrasion and the chemical treatments

tested. For a double lap shear specimen, the maximum obtainable strength was 920 kN/m (5250lb/in).

3. The stiffness of the patching material affects both the maximum strength of the adhesive layer and the overlap length required to attain this strength. For the double lap shear specimen, the higher stiffness (HS) patching material provided a maximum strength of 1030 kN/m (5900 lb/in) at a minimum overlap length of 50mm (2.0in).

4. The thickness of the steel adherend had an effect on the maximum obtainable strength. For the double lap shear specimen, the maximum strength obtained was only 670 kN/m (3825 lb/in).

Minford [3.3] lists other factors that affect the static strength and the durability of a joint: properties of the adhesive, interfacial imperfections, cure temperature, cure pressure, fillers, adhesive thickness, temperature, adhesive fracture resistance, adhesive fatigue resistance, and environment. These factors are not considered in this investigation.

3.6   REFERENCES

[3.1]   John, S.J., *"Predicting the Strength of Bonded Carbon Fibre/Epoxy Composite Joints"*, Composites Bonding, ASTM STP 1227, Dennis J. Damico, Thomas L. Wilkinson Jr., and Sandra L.F. Niks (ed.), American Society for Testing and Materials, Philadelphia, 1994, pp. 45-59.

[3.2]   Hart-Smith, L.J., *"Joints"*, Engineering Materials Handbook, Volume 1: Composites, ASM International, 1987, pp 479-495.

[3.3]   Minford, J.D., *"Adhesives"*, Durability of Structural Adhesives, Kinloch, A.J.(ed.), Applied Science Publishers Ltd., 1983, pp.135-214.

[3.4]   Mahoney, C.L., *"Surface Preparation for Adhesive Bonding"*, Handbook of Adhesives, Third Edition, Skeist, I. (ed.), van Nostrand Reinhold, 1990, pp. 74-93.

[3.5]   Baker, A.A., *"Crack Patching: experimental studies, practical applications"*, Bonded Repair of Aircraft Structures, Baker, A.A., and Jones, R. (ed), Martinus Nijhoff Publishers, 1988, pp. 107-173.

[3.6]   ASTM Designation D3528-92, *"Standard Test Method for Strength Properties of Double Lap Shear Adhesive Joints by Tension Loading"*.

[3.7]   Seiner, M.P., *"Stress Field Sensitivity of a Composite Patch Repair as a Result of Varying Patch Thickness"*, Composite Materials: Testing and Design (Tenth Volume), ASTM STP 1120, Glenn C. Grimes (ed.), American Society for Testing Materials, Philadelphia, 1992, pp. 444-464.

4.1   INTRODUCTION

A study of the structural integrity of the composite patch and the adhesive bond, described in chapters 2 and 3, is important for determining whether or not a bonded patch will fail under an applied static load. This is one aspect of this investigation; both the patch and the adhesive layer must be designed so that they will not fail under the maximum applied loads which are imposed upon them. The other part of this investigation is to study the effect that a sound patch has on a damaged steel adherend.

Using well known linear elastic fatigue crack propagation principles and the common precracked Compact Tension Specimen (CTS), this chapter first examines the effectiveness of a patch to retard the growth of a crack in a damaged pressure vessel. Patching is not an effective repair, however, on its own. A crack in a pressure vessel, patched or unpatched, imposes severe stress concentrations in the structure under applied loads. To increase the efficiency of the repair, both a patching repair and a removal of the severe stress concentration at the crack tip should be used. In another part of this chapter, the effectiveness of a patch to retard the initiation of a crack from a blunt-notched CT Specimen is investigated. Finally, in a practical application, the repaired structure must be able to withstand biaxial loading and retain pressure. The final part of this chapter examines the effectiveness of both patching and crack tip removal to repair a cracked cylindrical steel pressure vessel.

4.2   FATIGUE CRACK PROPAGATION

Fatigue crack propagation is defined in this investigation as the behaviour of a cracked structure under constant amplitude cyclic loading where the response of the structure is predominately elastic. Knowing the fatigue constants of the material, the geometry of the structure, the crack size, and the loading conditions, the rate of crack growth can be

predicted using fatigue mechanics. Two fatigue governing principles are particularly important in predicting crack growth behaviour: (1) the threshold stress intensity factor range, ΔK_{th}, and (2) the behaviour in the Paris regime. The threshold stress intensity factor range, ΔK_{th}, is the value of the ΔK where the crack growth rate, *da/dN*, ceases. If the applied ΔK is less than this value, a crack in a cracked structure will not propagate. If the applied ΔK is greater this value, the crack propagation is governed by the Paris regime of crack growth. The Paris regime is the stage in the crack propagation where the crack growth rate , *da/dN*, with respect to the stress intensity factor range, ΔK, is linear on a log-log scale. In the Paris regime, *da/dN* is expressed by the following equation (*C* and *n* are material properties):

$$da/dN = C(\Delta K)^n$$

(4.1)

This study investigates how a patch on a cracked structure affects the threshold value of the stress intensity factor range, ΔK_{th}, and the crack growth in the Paris regime.

4.2.1   The Compact Tension Specimen Design for Crack Propagation

The specimens employed to quantify the effect of patching on crack behaviour are standard ASTM CT fatigue specimens [4.1]. The CT specimen dimensions are shown in Figure 4.1. The CT specimen was fabricated from ASTM A-516 Gr 70 pressure vessel steel, a material commonly used in pressure vessel manufacture. The thickness of the specimen, *b*, is 15.9mm (5/8in), a thickness common to pressure vessel design. Two 12.7mm (0.5in) diameter holes were placed in the upper and lower corners to apply, through shear pin loading, a cyclic compressive or a cyclic tensile load to the specimen. A notch was machined into the specimen to provide a favourable location for the initiation of a crack.

To initiate a crack from the notch with minimal plastic damage at the crack tip, all CT propagation specimens were initially precracked in cyclic compression. Using a cyclic load of ±8.25 kN (±1850 lb) and a mean compressive load of 8.5 kN (1910 lb), each specimen was fatigued for one million cycles. Next, a compressive overload totalling 25.0 kN (5700 lb) was applied and upon resumption of the compressive cyclic load, a crack was initiated. To propagate the crack further, a cyclic load of ±2.38 kN (±535 lb) with a mean tensile load of 2.63 kN (590 lb) was used.
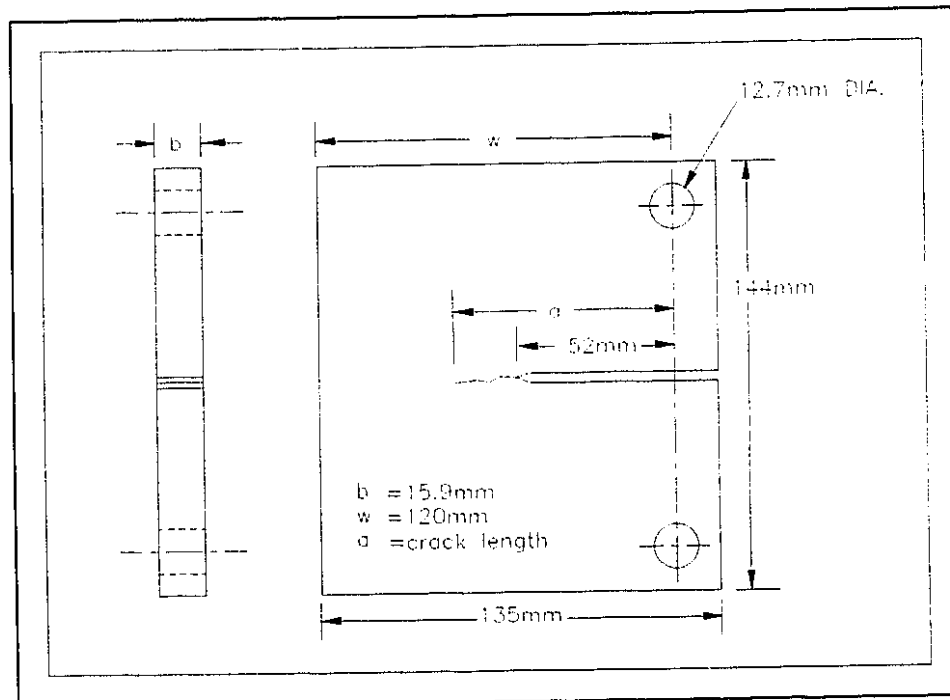
Figure 4.1: Compact Tension (CT) Fatigue Propagation Specimen

4.2.2   Measuring Crack Growth

Carbon fibre composite patches were placed on both sides of the cracked CT specimen to keep the loading symmetrical. Because the composite patches covered the crack, the crack growth could not be measured by visually monitoring the crack. A non-destructive

method for crack length determination had to be developed where visual techniques could not be utilized; a potential drop system was employed.

The potential drop method for crack length determination is based on the fact that as a crack propagates in a steel structure, the electrical resistance of the steel structure increases because the cross-sectional area of the steel structure is being reduced. Thus, by running a constant current through the specimen, and by measuring the electrical potential drop across the crack, the crack length can be determined. Figure 4.2 shows a schematic illustration of the potential drop system used in this investigation.
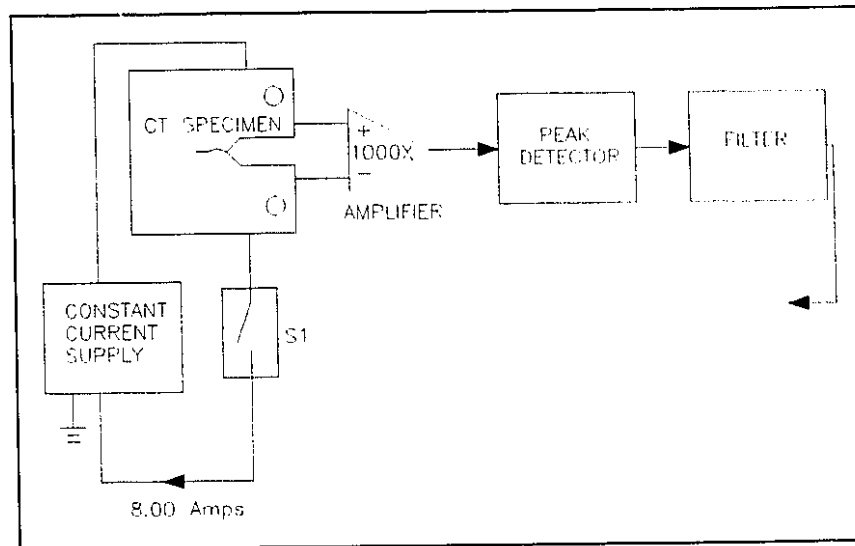
Figure 4.2: The potential drop measurement of the crack length.

Direct current is supplied to the specimen by way of a grounded constant current supply of 8.0 Amps through two leads at the top and the bottom of the specimen. Potential voltage leads are placed on either side of the crack to monitor the potential change as the crack propagates. In addition to the standard potential monitoring design outlined in [4.1], there are four additional features in this system:

1.   A 1000X amplification of the potential drop increases the signal to a magnitude which could be read by the data acquisition system. Next, the ASTM standard [4.1] suggests that the potential voltage readings should be taken at or near the peak load in the fatigue cycle to ensure that the crack is fully open when the potential reading is taken. In this set up, a peak detector was utilized. The peak detector takes a potential voltage reading when the crack is fully opened and stores this reading until a higher voltage results. A higher voltage can only be obtained if the crack has grown. Finally, a filter was placed at the output of the peak detector to filter out noise.

2.   The potential reading should be a function of the crack length only. Other electrical disturbances, such as a change in the resistance of the steel specimen due to changes in the local temperature, voltages produced by thermoelectric effects, and outside noise sources, could generate voltages in an order of magnitude similar to the potential readings generated by applying current through the specimen. Since these effects are present without a current through the specimen, a switch was introduced into the circuit. Every 5000 cycles, the switch (S1 on Figure 4.2) was turned off and then on and then off again with the potential drop being recorded at each switch setting. The net potential (the difference between the potential recorded when the current was on and the average potential when the current was turned off) is a function of the crack length only.

3.   The specimen was electrically insulated from the testing machine in order to ensure that the current travels through the CT specimen only. Two Delrin®[1] thermoplastic sleeves and four Delrin® thermoplastic washers separate the steel specimen from the testing grips so that current can not be routed through

---

1   Delrin® is a thermoplastic product manufactured by Johnston Industrial Products.

the grips and into the testing machine.

4.   A computer controlled data acquisition system was used in order to automate the recording of data. Every 5000 cycles, the mean load, the dynamic load, the potential drop across the crack when the current is switched on, and the potential drop when the current is switched off were recorded. The computer also controls the switch.

Figure 4.3 shows where the current leads and the potential leads are placed on the CT specimen. The position of the current and voltage leads in this particular specimen are so placed to *"reach a compromise between the sensitivity to changes in crack length (dP/da) and inconsistencies caused by small locational errors and other uncontrollable errors"* [4.2, p93]. Current leads and potential leads are fabricated using 2.0mm gauge copper wire and are welded to the specimen. The lead wires are twisted together to avoid any induced EMF voltages created by magnetic fields existing around the testing machine.
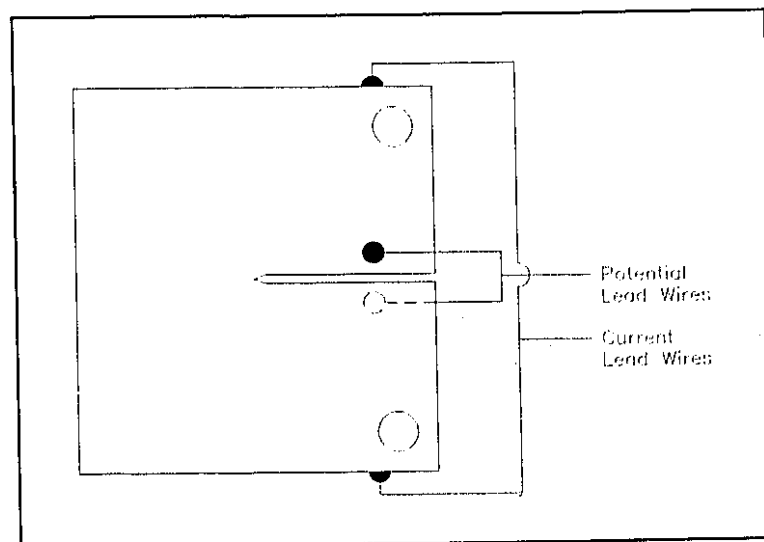
Figure 4.3: Location of potential and current lead wires on the CT specimen.

The relationship between the potential drop and the crack length ratio[2] is not linear but in the form of a third order polynomial. For this specimen geometry, a calibration curve (see Figure 4.4) was determined experimentally by measuring both the potential drop and the crack length of an unpatched specimen as the crack propagated. Note that the crack length was measured on each side of the specimen, using a replica tape, and the net crack length was taken to be the average of the two crack lengths measured. Note also that P_o is a term which normalizes the voltage reading. P_o was determined by measuring the potential drop reading at a known crack length and adjusting the reading accordingly so that the results fit the calibration curve. Using P_o accounts for variations of electrical properties between the different specimens and provides a single curve, independent of current and thickness. The calibration curve for this specimen geometry is:

$$a/w = -0.516979 + 1.61016(P/P_o) - 0.6995(P/P_o)^2 + 0.10895(P/P_o)^3 \qquad (4.2)$$
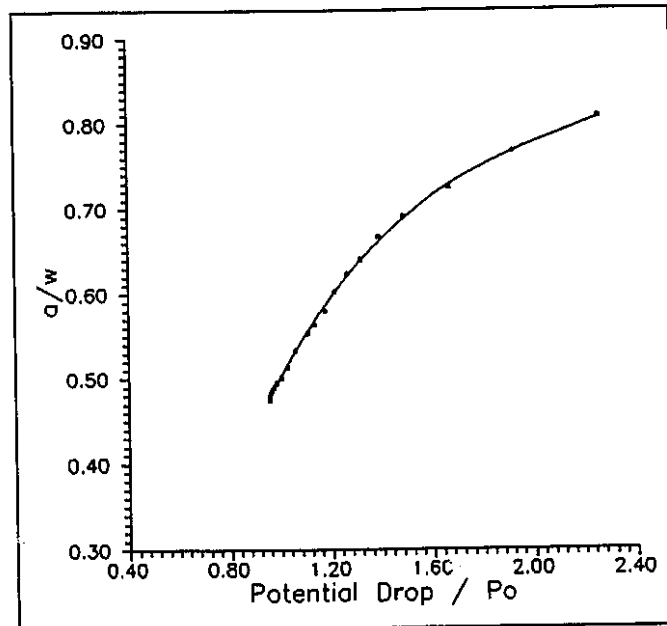
Figure 4.4: Potential Drop Calibration Curve

---

2   The crack length ratio, a/w, is the crack length, a, divided by the dimension, w (Figure 4.1).

4.2.3   Fatigue Crack Propagation in an Unpatched Specimen

After the precracking procedure was employed, the specimen was loaded with a mean tensile load of +2.63 kN (+590 lb) and a dynamic load of ±2.38 kN (±535 lb). Using the computer controlled data acquisition system, the potential drop readings were recorded every 5000 cycles. Figure 4.5 shows the normalized potential drop readings recorded over the life of the unpatched CT specimen, CTS1.
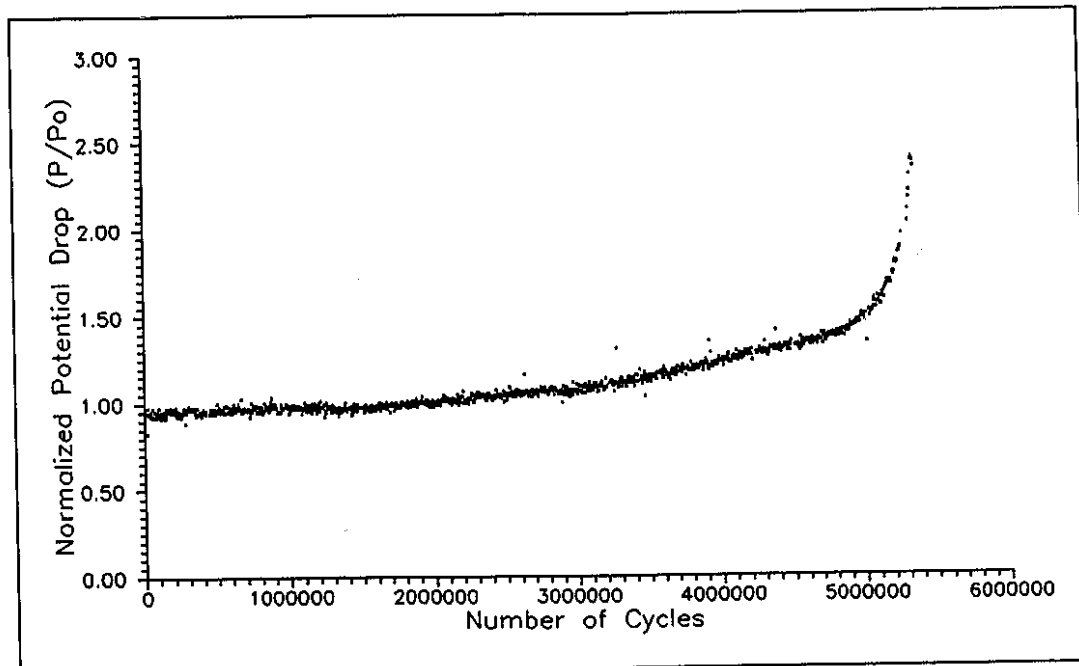
Figure 4.5: The normalized potential drop measured over the fatigue life of the unpatched specimen, CTS1.

Using the calibration equation for this specimen geometry (equation 4.2), the potential drop recordings can be converted to a crack length ratio, a/w, and plotted as a function of the number of cycles. Figure 4.6 shows the crack length ratio, a/w, as a function of the number of cycles. It is evident from Figure 4.6 that as the cyclic load continued to be applied to the specimen, the crack propagated. At 5,345,000 cycles, the crack length

60

ratio of the specimen was approximately 0.82 and the loading to the specimen was stopped.
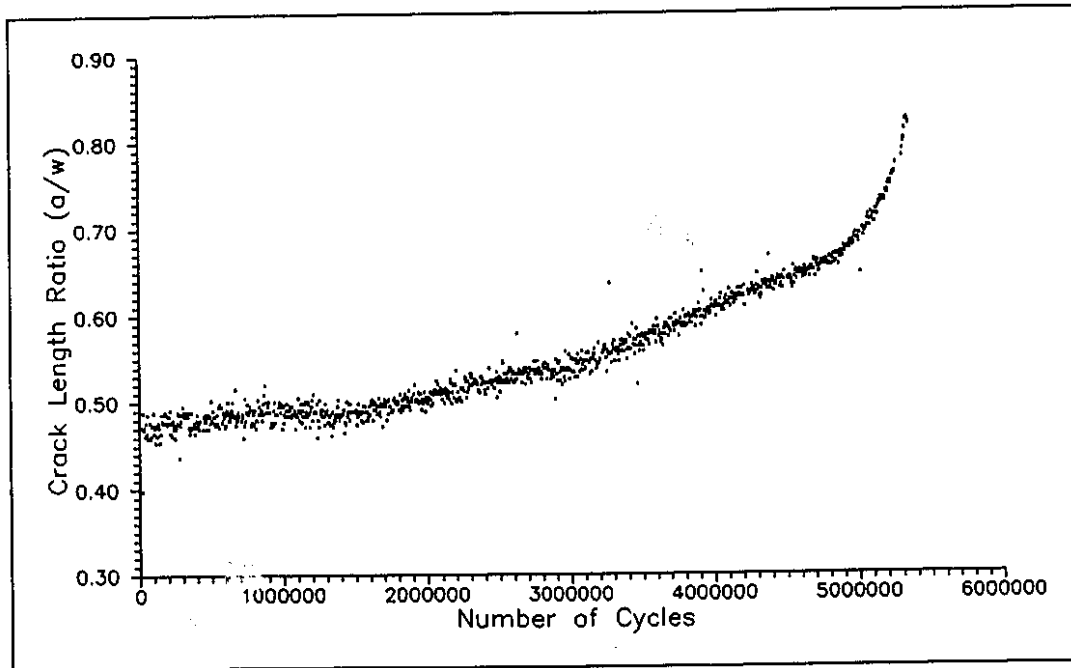
Figure 4.6: The growth of the crack length ratio, a/w, over the fatigue life of the unpatched specimen, CTS1.

An interesting parameter in fatigue mechanics which characterizes the propagation of cracks, is the crack growth rate, da/dN. From the relationship of the crack length ratio, a/w, verses the number of cycles, the crack growth rate, da/dN, can be determined. Appendix A details the numerical calculation of the growth rate, da/dN. Figure 4.7 shows the crack growth rate, da/dN, as a function of the crack length ratio, a/w. Two important crack growth regimes are illustrated: (1) At the crack length ratio of 0.485, the crack growth rate, da/dN, approaches zero. It appears that below this crack length ratio, the crack will not propagate. (2) At crack length ratios above 0.485, the crack propagates and its rate increases as the crack grows longer.
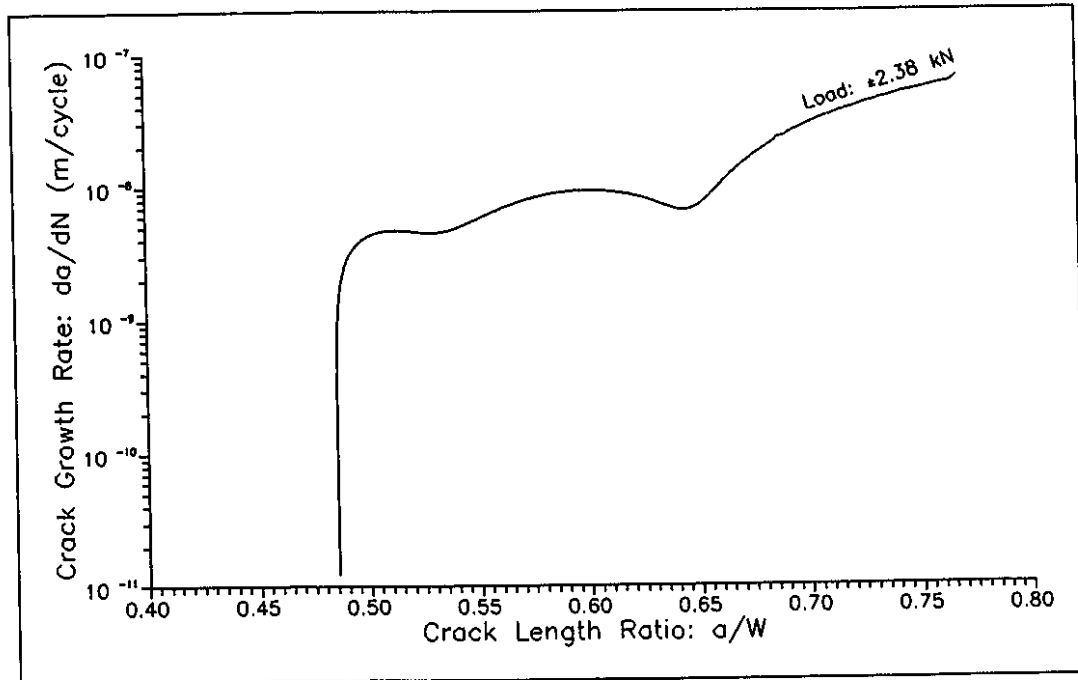
Figure 4.7: The crack growth rate, *da/dN*, in the unpatched specimen (CTS1) as a function of the crack length ratio, *a/w*.

Figure 4.8 illustrates the relationship of the crack growth rate, *da/dN*, with respect to the stress intensity factor range, ΔK. In this figure, the same two regimes are noted: (1) the threshold regime at a ΔK_{th} value of 8.0 MPa$\sqrt{m}$, and (2) the Paris regime which initiates with ΔK values above the threshold value. The crack growth rate in the Paris regime does not follow a linear relationship (dotted line) when plotted against the ΔK value on a log-log scale. As illustrated by the question mark in Figure 4.8, the crack growth seems to retard around a ΔK value of 14 MPa$\sqrt{m}$. The explanation for this deviation is unknown to the author (the specimen may have experienced a tensile overload during fatigue; or perhaps the specimen relaxed during machine down times under the sustained mean load). Despite this deviation, these values are in general agreement with the values published by Craig [4.3], and Ellyin and Li [4.4] also shown on the same figure.
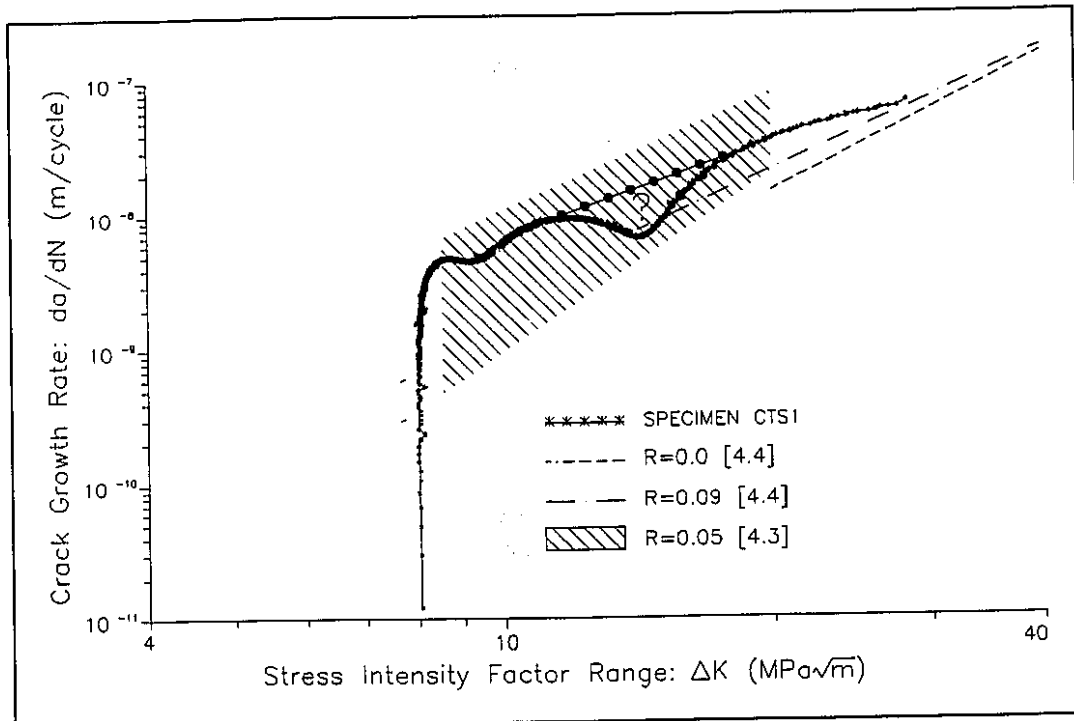
Figure 4.8: The crack growth rate, *da/dN*, in the unpatched specimen (CTS1) as a function of the stress intensity factor range, ΔK.

4.2.4   Fatigue Crack Propagation in a Patched Specimen

The CT specimen patching preparation and testing followed the following routine:

1.   After the crack initiation procedure was employed, the crack was allowed to grow in cyclic tension until the crack length, *a*, reached approximately 60mm.

2.   A patch was placed on both sides of the cracked CT specimen in order to keep the loading symmetrical. The patch had the following design: (1) the direction of the fibres were placed perpendicular to the direction of the crack, (2) the patch was tapered at the upper and lower ends in order to minimize the peel stresses in these areas, and thus, minimize potential debonding, (3) the patch geometry had a width of 60mm (2.4in) and an average length of

63

130mm (5.1in), and (4) the patch was placed so that its edge was at the tip of the machined notch. The patch was initially cured at room temperature (22°C (72°F)) for 3 days and then cured at 93°C (200°F) for 2 hours. The patch was then cooled back to room temperature.

3.   The patched CT specimen, CTS2, was then placed under the same cyclic tension-tension loading as the unpatched specimen, CTS1, and the crack growth was monitored using the potential drop system described above.

Figure 4.9 is a schematic illustration and Figure 4.10 is a photograph of the applied patch.
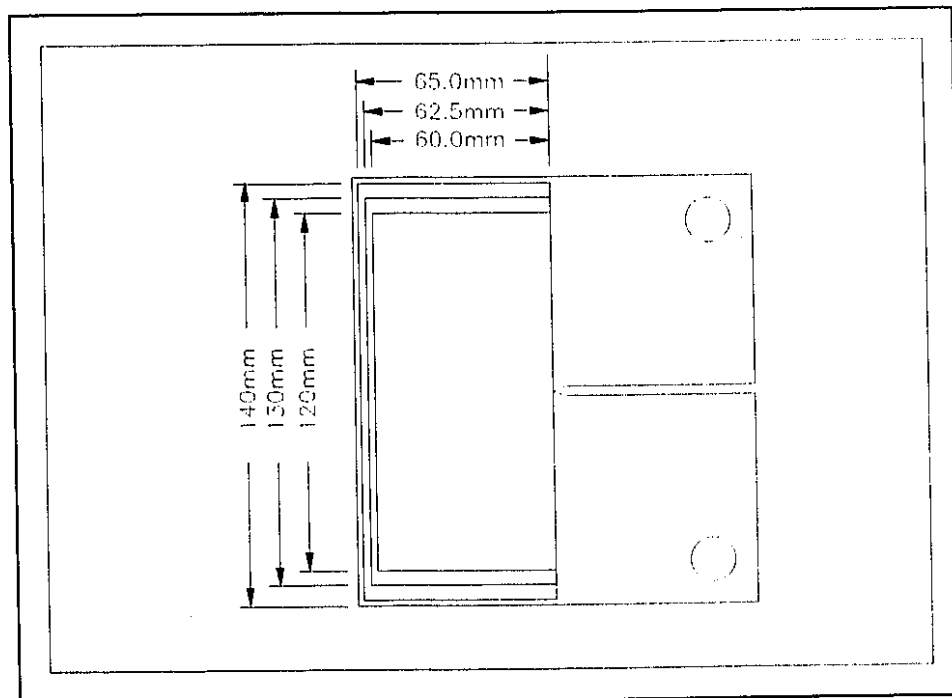
Figure 4.9: The patch geometry for the patched CT crack propagation specimen, CTS2.
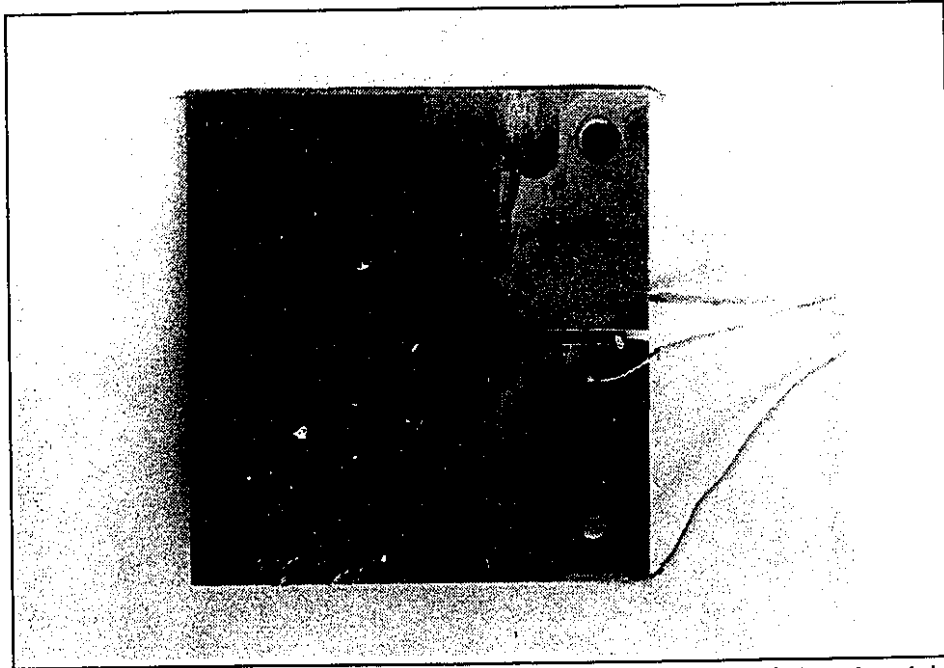
Figure 4.10: The patched propagation specimen showing both the applied patch and the current and potential lead wire locations.

For the patched specimen, CTS2, the crack did not propagate under the same loading conditions which caused the crack in the unpatched specimen, CTS1, to propagate. To propagate the crack, the dynamic load was increased 10% (to ±2.61 kN (±590 lb)), the mean load was increased 10% (to +2.89 kN (+650 lb)) and the specimen was cycled further. Under these increased loading conditions, the crack began to propagate. Figure 4.11 shows the normalized potential drop recorded as a function of the number of cycles. Figure 4.12 shows the crack length ratio as a function of the number of cycles. The results of the unpatched specimen, CTS1, are shown on the same figures for comparison purposes.
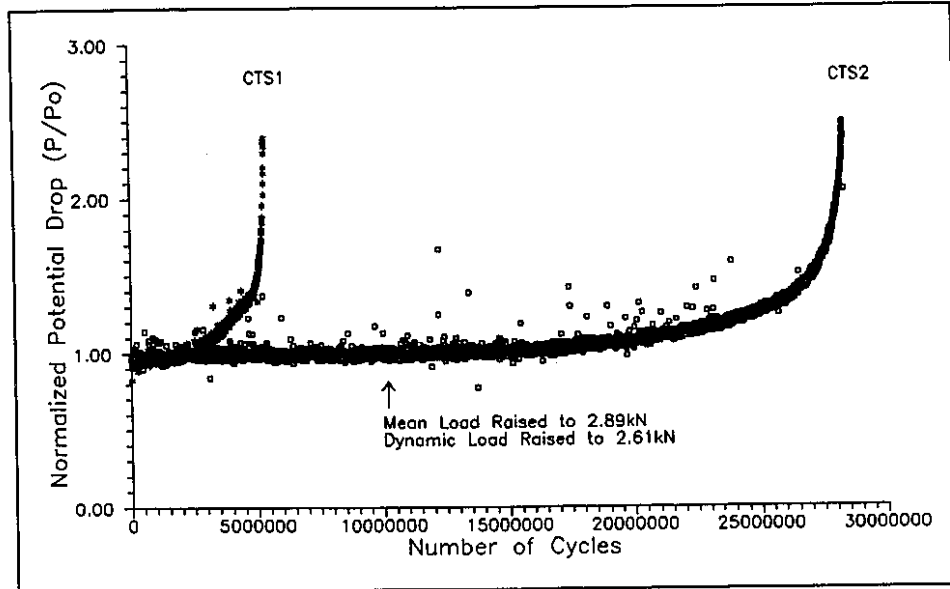
Figure 4.11: The normalized potential drop recorded over the life of the patched specimen, CTS2.
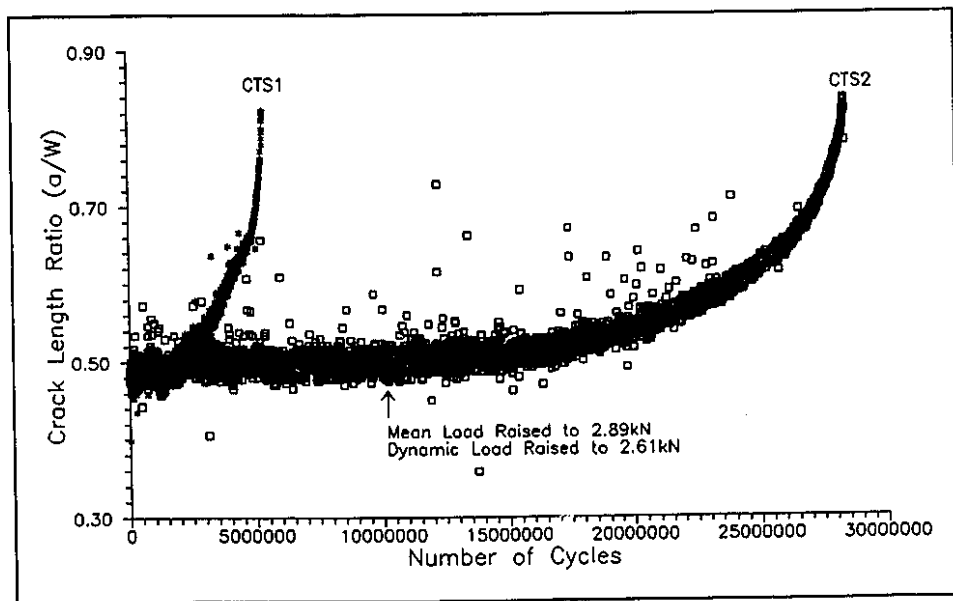
Figure 4.12: The crack length ratio, a/w, as a function of the number of cycles for the patched specimen, CTS2.

Figure 4.13 illustrates the crack growth rate, *da/dN*, as a function of the crack length ratio, *a/w*, for both the unpatched and the patched specimens.
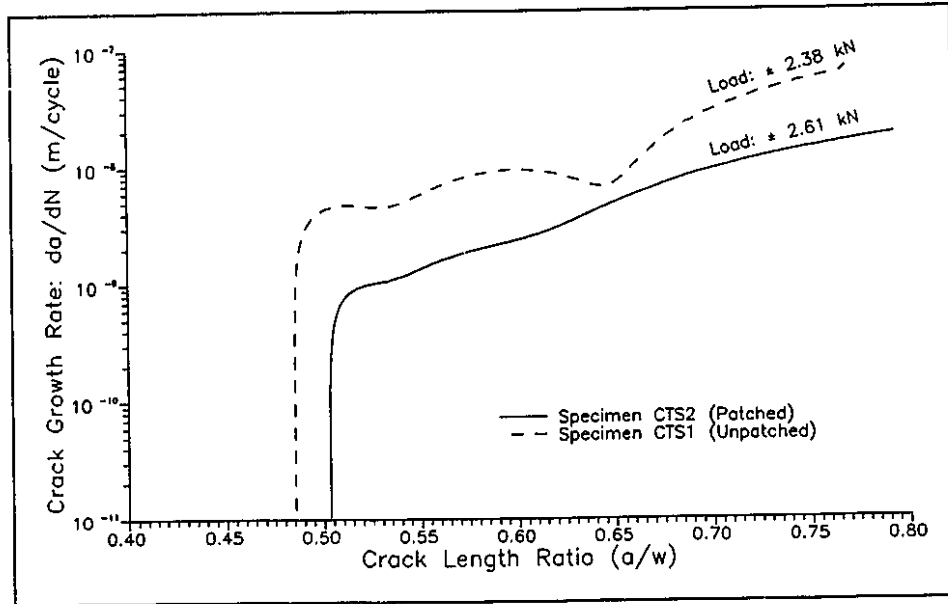
Figure 4.13: The crack growth rate, *da/dN*, of the patched specimen (CTS2) and unpatched specimen (CTS1) as a function of the crack length ratio, *a/w*.

Figure 4.13 illustrates that below the crack length ratio of 0.50, the crack in the patched specimen would not propagate whereas the crack in the unpatched specimen would, despite the higher applied load in the patched case. It is also evident that at crack length ratios above 0.50, the growth rate of the crack in the patched specimen is slower than the growth rate of the crack in the unpatched specimen, despite the higher applied load in the patched case. The patch slows the growth rate of the propagating crack and under certain conditions ($a/w < 0.5$, dynamic load $\leq \pm 2.61$ kN), arrests the crack altogether.

Figure 4.14 shows the crack growth rate, *da/dN*, of the patched and unpatched specimens as a function of the stress intensity factor range, ΔK. Note that the ΔK value for the patched specimen is based on the unpatched CTS geometry and is used, in this report,

for comparison purposes only. Because the ΔK value incorporates both the farfield applied load and the crack length into its formulation, it is practical for comparing the growth rates of the two different specimens.
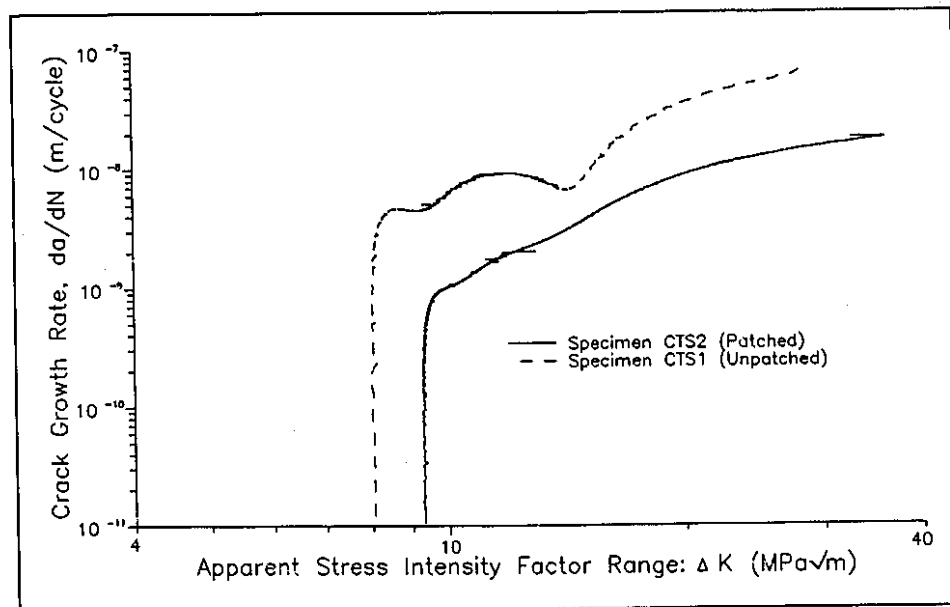
Figure 4.14: The crack growth rate, *da/dN*, of the patched specimen (CTS2) and the unpatched specimen (CTS1) as a function of the fluctuating stress intensity factor, ΔK.

The apparent threshold stress intensity factor range for the patched specimen is 9.5 MPa√m. Comparing this value with the unpatched configuration, it is observed that the threshold ΔK_{th} under which a crack will not grow is increased by 19% with the addition of a patch. It is also observed that in the Paris regime, the crack in the patched configuration grows slower under the same ΔK value. For this configuration, the patch reduced damage produced at the crack tip and extended the life of the cracked structure.

4.2.5   Debonding in a Patched Specimen

The amount of debonding in the adhesive layer was investigated by stripping the patch

from the adhesive layer. Baker [4.5] states that heating the patch at 190°C (374°F) for 2 hours discolours the debonded region by oxidation and allows for easy removal of the patch. Debonding, in the patched specimen, occurred between the adhesive layer and the steel adherend. Figure 4.15 illustrates the growth of the debonded area as the crack length grew from the notch. Baker [4.6] observed similar delamination in edge-notched aluminum specimens between the patch and the adherend. Baker described the delamination as a *"roughly triangular zone with its base at the edge of the panel and its apex at the tip of the crack"*. A similar shape is found here.
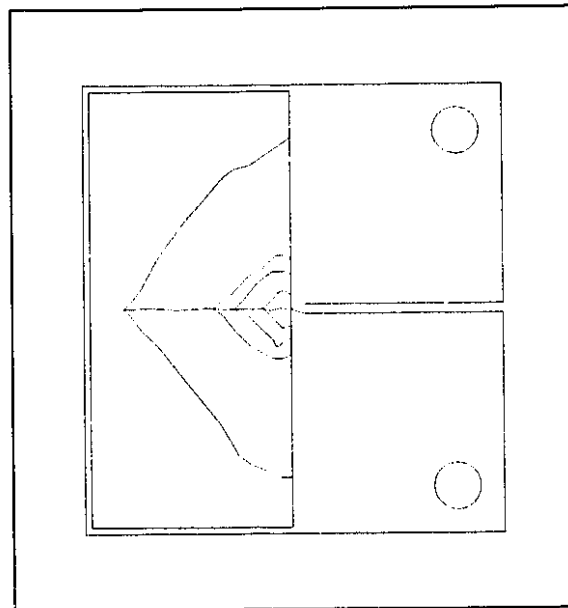
Figure 4.15: Debonding in the patched CT propagation specimen, CTS2.

The final length of the crack, *a*, was measured using magnetic flux resonance. The final crack length was measured to be 103mm. From the potential drop measurement, the crack length was recorded as being 100mm. The difference in these values arises because the specimen was loaded for another 5000 cycles after the last potential drop measurement was recorded.

4.3   FATIGUE CRACK INITIATION

A patch reduces the rate of crack propagation and under certain loading conditions, stops the crack from growing altogether. Despite this, a loaded cracked structure, patched or unpatched, represents a very dangerous design. In order to extend the life of a pressure vessel safely, the crack tip should be removed before the patching process is employed. One method of removing the crack tip is to drill a hole at the crack tip. This crack tip removal would reduce the severe stress intensity at the crack tip to a stress intensity more typical of a circular or elliptical hole. In terms of fatigue terminology, removing the crack from the loaded structure changes the crack behaviour problem from a fatigue crack propagation study to a fatigue crack initiation study. Fatigue crack initiation investigates the number of cycles required to initiate a crack from a smooth notch geometry.

4.3.1   The Compact Tension Specimen Design for Crack Initiation

The specimen used for the crack initiation studies has similar dimensions as the specimen used for the crack propagation studies but the notch geometry is different (see Figure 4.16). At a notch length, a, of 50mm (2.0in), a 3.2mm (⅛in) hole was drilled at the notch tip. It is assumed that a CT initiation specimen will provide similar results as a CT propagation specimen with a hole drilled at the crack tip. This assumption presumes that drilling a hole at the crack tip would remove all of the damage created by the crack during its propagation phase.

4.3.2   Measuring Crack Initiation

Crack initiation for this investigation is defined as the number of cycles required for the crack to start growing from the circular notch. In the unpatched specimen, the crack
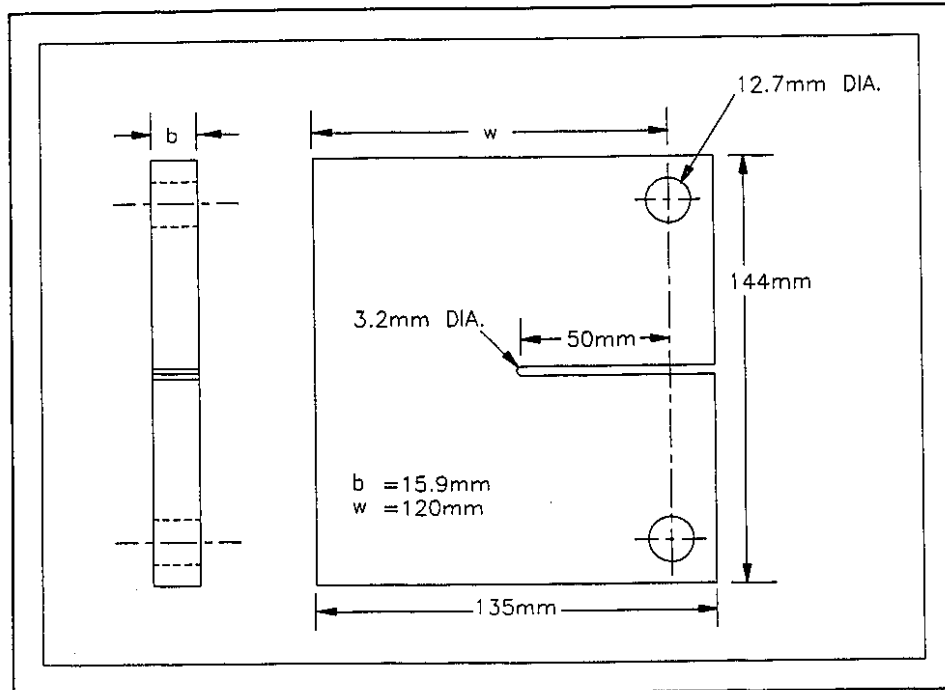
Figure 4.16: A Compact Tension (CT) Fatigue Initiation Specimen

growth is measured visually by monitoring the crack growth on both sides of the CT specimen. For the patched specimen, crack initiation is monitored by visually observing cracking through the notch and by monitoring the frequency of the load applied to the specimen. The testing machine loads the CT specimens through resonance principles; the frequency of loading is dependent on the stiffness of the specimen. Crack initiation changes the stiffness of the specimen and, thus, changes the frequency of the machine. After a crack initiates in the patched specimen, the crack length is determined by removing the patch.

4.3.3 Initiating a Crack in an Unpatched Specimen

The unpatched specimen, CTS5, was loaded in tension-tension cyclic loading with a tensile mean load of +8.9 kN (+2000 lb) and a dynamic load of ±8.1 kN (±1820 lb). The specimen had a fatigue initiation life of 2,149,000 cycles.

This value falls close to the value predicted using the S-N fatigue life curve for this material. Based on the applied load, F, the stress at the crack tip in the CT specimen, $\Delta\sigma_N$, is equal to the sum of the stresses created by the tension component of the applied load, F, and the bending stresses created by the applied load F:

$$\Delta\sigma_N = \Delta\sigma_{N(tension)} + \Delta\sigma_{N(bending)} \tag{4.3}$$

where:

$$\Delta\sigma_{N(tension)} = \frac{\Delta F}{[(w-a)b]} \tag{4.4}$$

and:

$$\Delta\sigma_{N(bending)} = \frac{6\Delta F(a + \frac{(w-a)}{2})}{(w-a)^2 b} \tag{4.5}$$

The circular hole drilled at the notch tip creates a stress concentration at this point. Wilson [4.7] provides a stress concentration factor, K_t, for blunt notched CT specimens. This estimation, based on finite element analysis, relates the stress intensity factor to the notch sharpness and the remaining ligament length. For the specimen geometry tested, the stress concentration factor was estimated to be 3.90[3]. Using this value, the corrected stress, $\Delta\sigma_T$, at the notch tip is equal to:

$$\Delta\sigma_T = \Delta\sigma_N K_t \tag{4.6}$$

The value of $\Delta\sigma_T$ in this case assumes that the material is responding in a linear elastic

---

3   Note that discrepancies will exist in the results. The calculations in reference [4.7] were based on an *a/w* ratio of 0.4375 whereas experimentally, the *a/w* ratio was only 0.42.

manner. The value of $\Delta\sigma_T$ is never reached, however, because the material plastically deforms above its yielding limit. Using an energy approach, Ellyin and Kujawski [4.8] postulated that the actual stress range at the crack tip, $\Delta\sigma$, can be calculated by equating the theoretical energy of one loading cycle using the value $\Delta\sigma_T$ and assuming an elastic response and the hysteresis energy of the elastic-plastic cyclic response:

$$\frac{\Delta\sigma_T^2}{2E}=\frac{1}{(1+n')}\Delta\sigma\Delta\epsilon^P+\frac{\Delta\sigma^2}{2E} \qquad (4.7)$$

where n' is the cyclic strain-hardening exponent and the plastic strain range, $\Delta\epsilon^P$, is determined from the cyclic stress-strain relation:

$$\Delta\epsilon^P=2\left(\frac{\Delta\sigma}{2K'}\right)^{1/n'} \qquad (4.8)$$

where K' is the cyclic strength coefficient. The S-N curve for this material is [4.9]:

$$\frac{\Delta\sigma}{2}=903.3\,(N_f)^{-1.02} \qquad (4.9)$$

where N_f is the number of cycles to failure. Using equation 4.9 and knowing $\Delta\sigma$ from equations 4.7 and 4.8, the theoretical number of cycles to failure, N_f, for this material is calculated to be approximately 2,100,000 cycles. This compares well to the measured value of 2,149,000 cycles.

4.3.4   Initiating a Crack in a Patched Specimen

Figure 4.17 and Figure 4.18 show the dimensions of a patch applied to the notched CT specimen. The patch was placed on both sides of the specimen with its fibres orientated parallel to the direction of the applied load. The patch was designed to cover the areas

both in front of and behind the notch so that the mechanisms of load transfer and notch bridging could both be utilized. The patch was tapered at each end so that peeling stresses would be minimized.

Initially, the patched specimens were loaded at the same load level as the unpatched specimen. The patched specimens were loaded in tension-tension cyclic loading with a mean tensile load of $+8.9$ kN ($+2000$ lb) and a dynamic load of ± 8.1 kN (± 1820 lb). Where the unpatched specimen failed in this loading range, the patched specimens did not initiate a crack after 10 million cycles. For each specimen, the dynamic and mean loads were increased by intervals of approximately 5% (keeping the R-ratio at 0.05) until a crack was initiated.
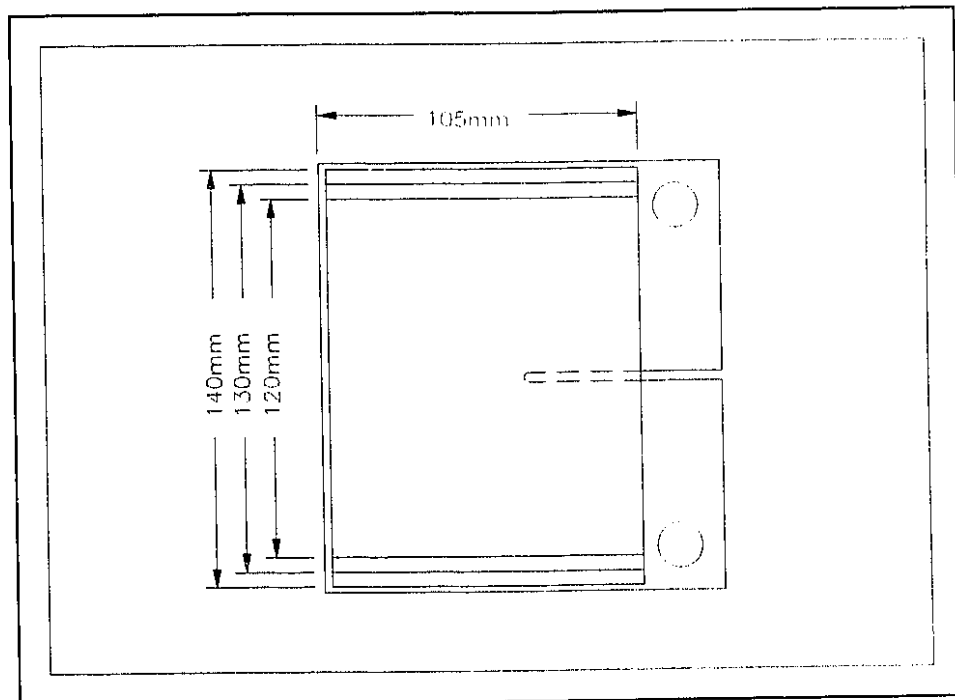
Figure 4.17: The patch geometry for the CT Initiation Specimen.
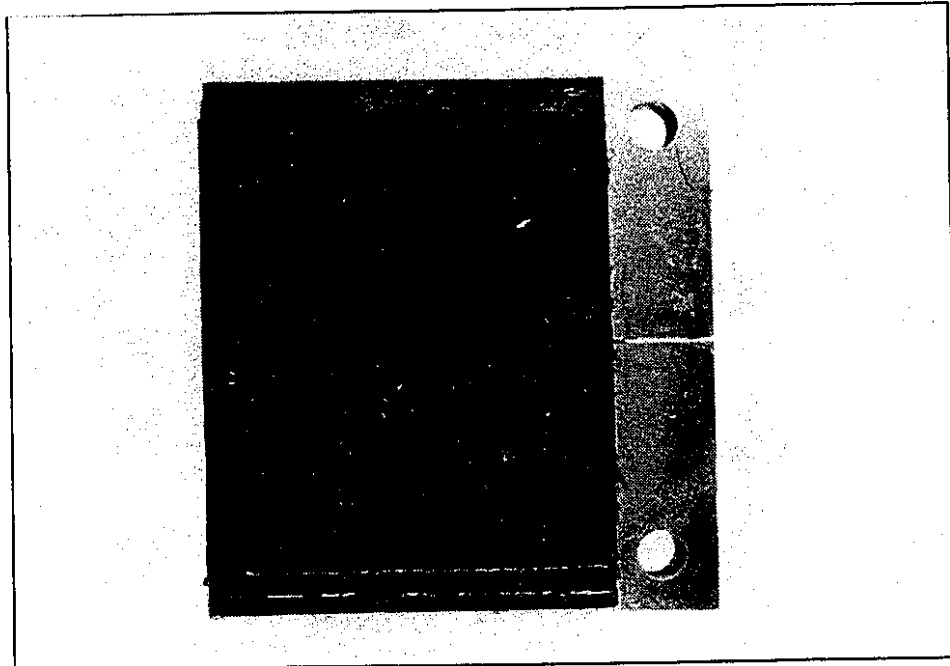
Figure 4.18: A CT Initiation Specimen with an applied patch.

Four different patched CT initiation specimens were investigated:

1. CTS6 had three layers of lower stiffness (LS) carbon fibre composite material on each side of the specimen. The surface was prepared by hand grinding with 80 grit sandpaper and cleaned by using an acetone wipe.

2. CTS7 had three layers of lower stiffness (LS) carbon fibre composite material on each side of the specimen. Sandblasting was used to prepare the steel surface.

3. CTS8 had six layers of lower stiffness (LS) carbon fibre composite material on each side of the specimen. Sandblasting was used as the surface preparation technique.

4. CTS9 had three layers of higher stiffness (HS) carbon fibre composite material on each side of the specimen. The steel surface was also sandblasted in preparation for bonding.

Table 4.1 presents the results for the CT initiation specimens. With each specimen, the loading history, the cycles to initiation, and the crack length[4] at initiation were recorded.

	Surface Preparation	Mean Load	Dynamic Load	Cycles to Initiation	Crack Length at end of test
CTS5:Unpatched		8.9kN	±8.1kN	2,150,000	1.0mm
CTS6:3lyrs:LS	sandpaper	8.9kN	±8.1kN	10,000,000+	
		9.5kN	±8.6kN	10,000,000+	
		10.0kN	±9.0kN	2,000,000	2.4mm
CTS7:3lyrs:LS	sandblast	8.9kN	±8.1kN	10,000,000+	
		9.5kN	±8.6kN	10,000,000+	
		10.0kN	±9.0kN	10,000,000+	
		10.5kN	±9.5kN	2,000,000	N/A
CTS8:6lyrs:LS	sandblast	8.9kN	±8.1kN	10,000,000+	
		9.5kN	±8.6kN	10,000,000+	
		10.0kN	±9.0kN	10,000,000+	
		10.5kN	±9.5kN	10,000,000+	
		11.0kN	±9.9kN	160,000	29.0mm
CTS9:3lyrs:HS	sandblast	8.9kN	±8.1kN	10,000,000+	
		9.5kN	±8.6kN	10,000,000+	
		10.0kN	±9.0kN	7,000,000	13.5mm

Table 4.1: Loading history and initiation loads of the CT Initiation Specimens.

Patching increases the load required for crack initiation. When loaded with a tensile mean load of +8.9 kN (+2000 lb) and a dynamic load of ±8.1 kN (±1820 lb), a crack did not initiate in specimen CTS6 after 10 million cycles. It is assumed that if a crack does not initiate after 10 million cycles, the specimen is loaded below its fatigue endurance limit and a crack is not going to initiate at this load level. For this specimen, the dynamic load was raised to ±8.6 kN (±1930 lb) and then raised again to ±9.0 kN

---

4   The crack length at initiation was determined by removing the patch.

($\pm$2020 lb) before a crack initiated and propagated to a length of 24.0mm (0.94in).

Specimen CTS7 had the same patch geometry as specimen CTS6 but used a different surface preparation technique on the steel. Despite the same patch geometry, the specimen CTS7 had to be loaded to an even higher load level before a crack was assumed to have initiated. Upon removal of the patch, a crack could not be observed using magnetic flux or microscopic examination. This indicates that the specimen could have been loaded further. This finding is consistent with previous findings on surface preparation and double lap shear specimens (sec 3.4.2). Previous investigations stated that the sandblasting technique provided a stronger bond than hand grinding with sandpaper. Here the sandblasting technique provided a more durable repair.

Specimen CTS8 used 6 layers of the patching material instead of 3 layers on each side of the specimen. This specimen produced the best repair; this specimen was able to withstand the largest amount of applied load before initiating a crack. From this result, it can be concluded that a thicker patch provides a more efficient repair.

Specimen CTS9 used 3 layers of the higher stiffness (HS) patching material. Despite the fact that the patching material had a higher stiffness than specimen CTS7, the specimen initiated a crack at a lower load level. This result could be attributed to the fact that the total thickness of the patch in specimen CTS9 was less than the thickness of the patch in specimen CTS7.

4.3.5 Debonding in the Patched Specimens

Thermal stripping was used to remove the patches and examine the debonding in the adhesive layer. Figure 4.19 shows the degree of debonding observed on one side of each of the patched CT initiation specimens. The shaded areas in the figure indicate the

degree of debonding that occurred just prior to crack initiation.

a) Debonding in the CT initiation
specimen, CTS6.

b) Debonding in the CT initiation
specimen, CTS7.

c) Debonding in the CT initiation
specimen, CTS8.

d) Debonding in the CT initiation
specimen, CTS9.
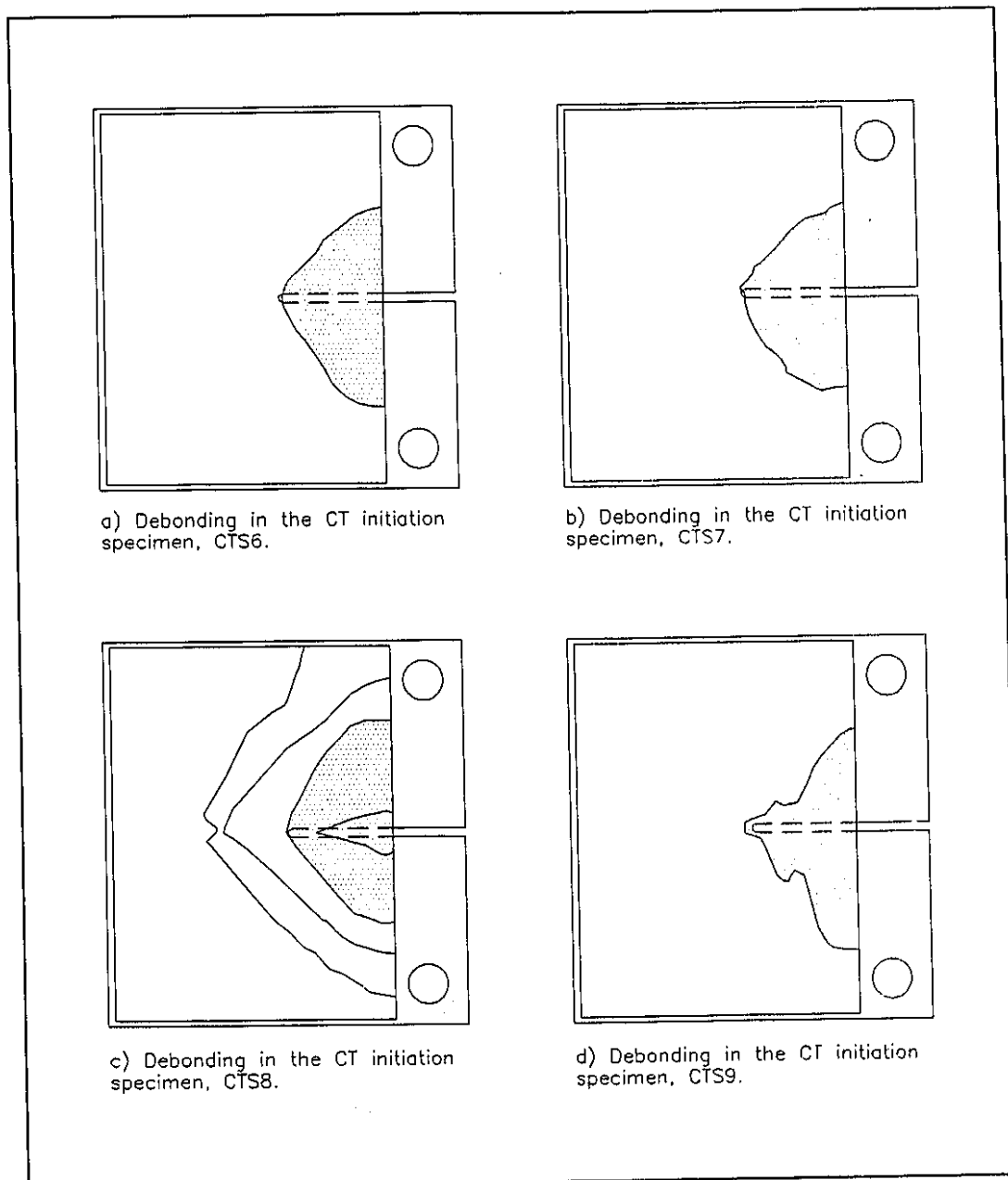
Figure 4.19: Debonding in the CT Initiation Specimens. The shaded areas represent debonding prior to crack initiation. The contour lines (Figure 4.19c) represent debonding after the crack propagated.

For the CT specimens patched with the lower stiffness (LS) composite (CTS6, CTS7, and CTS8), the debond area prior to initiation is similar in shape and size. It appears that there is some critical debond size that develops prior to crack initiation for these specimens. Perhaps this critical debond area must be attained before crack initiation. Perhaps the load patterns in the patched steel CT specimen encourage debonding in this shape and size. Baker [4.6] observed a retardation effect in patched panels with long edge cracks ($a > 25$mm). This researcher noted that under constant amplitude cyclic loading, the crack propagation of a long crack was delayed whereas the crack propagation in a short crack ($a < 5$mm) started immediately under an applied load. Baker attributed this delayed propagation to the patch reducing the stress intensity, ΔK, at the crack tip. The author speculates that perhaps this retardation is also a function of the debond growth in the adhesive layer. The size of the debond area affects the applied stress intensity factor range, ΔK, in the cracked CT specimens. A similar phenomena would take place in the CT initiation specimens. Under an applied cyclic load, the debond area would grow and increase the stress range, $\Delta \sigma$, at the notch tip. Future work is needed to support these conclusions.

Figure 4.19c shows the growth of the debond area before and after crack initiation in specimen CTS8. Baker [4.5] found that the. is a positive correlation between the crack growth rate and the amount of debonding in the adhesive layer. In these initiation specimens, debonding would have a similar affect. In specimen CTS8, the debond grew to a critical size before a crack initiated in the specimen. After initiation, the debond area grew as the crack grew until the loading to the specimen was stopped. The failure in the specimen was a combination of the crack propagation and the debonding in the adhesive layer.

Figure 4.19d shows the debonded area in the higher stiffness (HS) material. For this material, the debond area prior to initiation is different in shape than the areas observed

in the lower stiffness (LS) repairs. The higher stiffness material seems better able to resist debonding under cyclic loading. Further experimental analysis is needed to support this conclusion.

4.4 PRESSURE AND BIAXIAL LOADING

The CT specimen quantifies the effectiveness of a patch in terms of crack initiation and crack propagation in steel. A different specimen is needed, however, to investigate the effectiveness of a repair on a pressurized vessel with biaxial loading.

Loading in a pressure vessel is different from loading in the CT specimens. Initially, a pressure vessel has principle loading in two directions; the layers in the patch must be placed so that sufficient load is transferred in each direction and splitting does not occur between the fibres. Secondly, the curvature of the pressure vessel has an effect on the stresses at the crack; curvature increases the applied stress intensity factor, ΔK. Finally, in a cracked vessel, the radial stresses caused by the internal pressure causes the wall of the vessel to protrude outwards. Each of these variables cause both an increase in the stress intensity at the crack tip and a more complicated loading on the patch.

4.4.1 Biaxial Test Specimen Design

The specimens used for this part of the investigation were chosen from previous in-house investigations of biaxial fatigue. Each specimen was machined from ASTM A-516 Gr 70 steel. Each specimen had a cylindrical test section which could be pressurized and pulled axially in order to created a desired loading ratio between the hoop and axial axis. From previous investigations, the cylindrical specimens were cracked ($a \approx 3.5$mm) along a direction parallel to the axial axis of the specimen and considered to have failed because the specimens could not retain pressure. The specimen is shown in Figure 4.20.

Figure 4.20: The Biaxial Fatigue Specimen

4.4.2   Pressure and Biaxial Loading in a Patched Structure

Static Loading

For the first test, the stress concentrations at each end of the crack were removed by drilling a 0.79mm (0.031in) hole at each crack tip. The rest of the crack was gouged out in the shape of a V-groove. Because of pressure, a plug must be used in the drilled holes and the V-groove to prevent the escape of fluid.   For these specimens, the displaced material was replaced by using a 50% tin 50% lead solder. It should be noted here that the use of the solder technique is not intended to be the plug material in a pressure vessel application, but for this specimen size and loading condition, the lead-tin solder is effective. A practical plug material still needs to be investigated.

The biaxial specimen which was repaired by drilling holes at the crack tip and by

plugging the holes with solder was monotonically loaded with internal pressure until failure. Failure in the biaxial specimens was indicated by leakage of pressurized fluid. Using the biaxial specimen without a patch but with the soldering plug, the specimen was loaded to an internal pressure of 11.8 MPa (1710 psi). This failure load corresponds to a hoop stress, σ_h, of 255 MPa (37.0 ksi) and an axial stress, σ_a, of 127 MPa (18.5 ksi). Failure occurred because the crack opened and fluid escaped around the plug material.

The next test used holes at the end of the crack tips, a lead-tin solder plug, and a patch to repair the vessel. The patch employed the use of 3 layers of unidirectional carbon fibre wound around the cylinder in the hoop direction. The patch was 20mm (0.8in) wide, 85mm (3.3in) long, and was not permitted to overlap on the opposite side of the vessel. The failure pressure of the patched and plugged specimen was 23.3 MPa (3384 psi) which corresponds to a hoop stress, σ_h, of 500 MPa (75.5 ksi) and an axial stress, σ_a, of 250 MPa (37.8 ksi). Failure in the patched pressure vessel occurred through debonding of the patch from the steel surface. When the patch was removed, the soldered crack opened and fluid escaped.

	Failure Pressure	Failure Hoop Stress, σ_h	Failure Axial Stress, σ_a
Unrepaired	0 MPa	0 MPa	0 MPa
Holes and Plug	11.8 MPa	255 MPa	128 MPa
Holes, Plug and Patch	23.3 MPa	500 MPa	250 MPa

Table 4.2: The static failure loads of the repaired Biaxial Specimen.

Cyclic Loading

In this experiment, the cracked specimen was again repaired by drilling holes at the end of the crack tip, filling the displaced material with a tin-lead solder, and patching the

specimen with a patch similar to the patch applied in the static test. After the application of the patch, the specimen was loaded with a constant amplitude fully reversed (R = -1) equibiaxial cyclic stress, $\Delta\sigma_h = \Delta\sigma_a$, of 500 MPa until failure. An original undamaged biaxial specimen would survive approximately 10.000 cycles under this loading. With the repair, the specimen lasted 2135 cycles before the leakage was detected in the specimen. The specimen failed because the solder plug cracked and fluid escaped. A minimal amount of debonding had occurred prior to failure in the adhesive layer in an elliptical shape around the crack.

There are some problems with this cyclic loading investigation. Firstly, the loading in the specimen was a high-stress low-cycle fatigue loading. In a practical pressure vessel application, the imposed cyclic loading would not be this severe. Secondly, the cyclic loading to the biaxial specimen was fully reversed. In a practical pressure vessel application, the pressure vessel would be under tension-tension loading.

This section on biaxial and pressure loading had two purposes: (1) to determine if the repair of a specimen subjected to biaxial loading and pressure loading is feasible, and (2) to point out future research in biaxial testing. From the results, it can be concluded that a pressure vessel with a through-thickness crack can be repaired by removing the crack tip, plugging the holes, and patching. This repair can withstand a certain degree of static and cyclic loading.

4.6   CONCLUSIONS

The following conclusions are derived from investigations examining the effect of a patch repair on CT propagation specimens, CT initiation specimens and biaxial specimens:

1.   Using standard CT propagation specimens, the effect of a carbon fibre

composite patch on crack propagation in steel was determined. The potential drop system shown in Figure 4.2 was effective in measuring the crack length for both the patched and unpatched specimens. It was observed using the potential drop system that a patch was effective in reinforcing the cracked steel structure. A patch with the dimensions shown in Figure 4.9 increased the estimated value of ΔK_{th} from 8.0 MPa$\sqrt{m}$ to 9.5 MPa$\sqrt{m}$. A patch also reduced the growth rate in the linear regime of patch growth.

2. A more efficient repair of a cracked structure involves a combination of drilling a hole at the crack tip to reduce the stress concentration and patching. Removing the crack tip changes the problem from a crack propagation problem to a crack initiation problem. As a result, the applied loads required to induce damage in the structure are much higher.

3. Debonding is a factor in determining the efficiency of patch repair. Debonding develops in the adhesive layer and grows with applied cyclic loading. The debonded area is concentrated in the wake behind the crack tip but exists at the crack tip as well.

4. The repair scheme involving both the removal of the crack tip and patching can be applied to a pressure vessel. Using biaxial specimens it was shown that this repair technique was able to withstand some amount of biaxial and pressure loading.

4.7 REFERENCES

|4.1| ASTM Designation E647-91, *"Standard Test Method for Measurement of Fatigue Crack Growth Rates"*.

|4.2| Hicks, M.A., and Pickard, A.C., *"A Comparison of Theoretical and Experimental Methods of Calibrating the Electrical Potential Drop Technique for Crack Length Determination"*, International Journal of Fracture, Vol. 20, 1882, pp. 91-101.

[4.3]   Craig, D.F., *"Growth and Behaviour of Short Cracks in Ferritic/Pearlitic Steel"*, Master of Science Thesis, Department of Mechanical Engineering, University of Alberta, 1994.

[4.4]   Ellyin, F. and Li, H.P., *"Fatigue Crack Growth in Large Specimens With Various Stress Ratios"*, Journal of Pressure Vessel Technology, Vol. 106, August, 1984, pp. 255-260.

[4.5]   Baker, A.A., *"Repair Efficiency in Fatigue-Cracked Aluminum Components Reinforced with Boron/Epoxy Patches"*, Fatigue and Fracture of Engineering Material Structures, Vol. 16, No. 7, 1993, pp. 753-765.

[4.6]   Baker, A.A., *"Fibre Composite Repair of Cracked Metallic Aircraft Components - Practical and Basic Aspects"*, Composites, Vol. 18, No. 4, September, 1987, pp. 293-308.

[4.7]   Wilson, W.K., *"Elastic-Plastic Analysis of Blunt Notched CT Specimens and Applications"*, Journal of Pressure Vessel Technology, November, 1974, pp. 293-298.

[4.8]   Ellyin, F. and Kujawski, D., *"Generalization of Notch Analysis and its Extension to Cyclic Loading"*, Engineering Fracture Mechanics, Vol. 32, No. 5, 1989, pp. 819-826.

[4.9]   Lefebvre, D. and Ellyin, F., *"Cyclic Response and Inelastic Strain Energy in Low-Cycle Fatigue"*, International Journal of Fatigue, Vol. 6, No. 1, 1984, pp. 9-15.

5.1 INTRODUCTION

Investigating the effectiveness of applying a patch on a damaged steel structure is complex. Unfortunately, loading patterns in the patch, the adhesive bond, and the cracked steel structure are not easily determined. The loading in the structure is dependent on the size and orientation of the damage, the material properties and geometry of the steel adherend, the strength of the adhesive bond that adheres the patch to the damaged structure, and the material properties and geometry of the applied patch. As a result of these variables, designing a patch to repair a damaged pressure vessel is difficult and cannot be precisely determined without sophisticated numerical calculations.

Despite this, the purpose of this investigation was to provide an understanding of the mechanisms involved in the patching repair of a damaged pressure vessel, to provide some material properties and basic strength results for the particular steel/composite system used in this application, and to determine whether patching is a feasible alternative for the repair of damaged pressure vessels.

5.2 PATCH DESIGN PARAMETERS

There are certain design variables which must be addressed when designing a patch for a damaged pressure vessel:

(1)   The cure temperature of the composite patch and the adhesive bond affects the strength of the bonded structure. Strong room-temperature curing materials would be the optimal choice for repair. As one argument, any cure temperature above room temperature would start to cause residual compressive stresses in the patch and tensile stresses in the bond. After the curing cycle is applied and the bonded structure is cooled back to room

86

temperature, the differences in the coefficients of thermal expansion between the steel and the composite patch would cause the steel to contract more than the composite patch. Using room-temperature curing materials would avoid this difference in contraction upon cooling. Also, employing a room-temperature curing patch and adhesive would be practical. Without the need for heat, there would be no difficulty in applying the patch to a pressure vessel that is in service. Despite these advantages, finding a room temperature curing composite with sufficient strength requirements for a pressure vessel application is difficult. Typically, a higher curing temperature provides more strength to the composite structure.

For this composite material and epoxy adhesive, the maximum shear strength between the composite laminae layers was obtained when the composite was cured at 93°C (200°F) for 2 hours. Because of this relatively low cure temperature, the heat could easily be applied with a heating pad or a heat gun. As a results, only a small localized area on the pressure vessel's surface will be heated by the cure cycle of the composite patch. Because the surrounding steel structure is cool, the thermal expansion of the steel with the addition of heat is constrained and the residual stresses in the steel upon cooling are reduced.

(2)   The design of the patch determines the loading patterns from the steel structure to the patch, the amount of load that will be transferred to the patch, and whether or not the patch will fail under an applied load.

The tensile stiffness of the applied patch and stresses in the adhesive layer:

The stiffness and thickness of the patch determine the load transfer patterns

from the steel to the patch, and as a result, affect the stresses imposed on the adhesive bond. In section 3.2.3, it was discussed that the strength of the bond of a double lap shear specimen increased when the product of the tensile stiffness and the thickness of the composite, $E_c t_c$, approached the product of the tensile stiffness and thickness of the steel, $E_s t_s$:

$$E_c t_c \rightarrow E_s t_s \qquad (5.1)$$

In a practical pressure vessel repair, not all of the applied load is transferred to the patch as part of the load is still supported by the cracked vessel. Also in a pressure vessel repair, the ends of the patch are tapered. Factors such as these cause the relation in equation 5.1 no longer hold true. In practical design consideration, however, the thickness of the pressure vessel will be much larger than the thickness of the composite patch:

$$t_s \gg t_c \qquad (5.2)$$

As a result, choosing the stiffest available material will provide the best design in terms of bond load distribution. Despite this, a stiffer material would transfer more load away from the cracked steel and through the adhesive bond. Choosing the stiffest available material will also place a greater load on the adhesive bond. The optimal patch design in terms of tensile stiffness and thickness is indeterminate using simple analysis. A numerical investigation would have to be employed.

The tensile stiffness and the effectiveness of the repair:

The tensile stiffness and thickness of the applied patch also determine the efficiency of the repair. Assuming a fully bonded patch, the stiffest patching

material would transfer the most load away from the cracked structure and work well at pulling the crack closed.

The ultimate strength of the applied patch:

The ultimate strength of the composite patch determines whether or not the patch will fail under an applied load. For composite materials, the material is strongest and most stiff when loaded in the direction parallel to the direction of the fibres.

The overlap length of the applied patch:

The overlap length is also important. There is a minimum overlap length required to obtain the maximum load transfer capabilities of the bond. Beyond this value, no more load can be transferred by the structure.

(3)   The surface of the steel must be prepared for bonding with the epoxy adhesive. For steels, surface preparation consists of the removal of the old contaminated surface layer and the formation of a fresh oxide layer for bonding. In this investigation, the surface erosion (sandblasting) technique provided the strongest bond between the steel and the composite patch.

(4)   Patching a cracked steel structure increases the threshold load below which cracks would not propagate and decreases the growth rate of propagating cracks. To increase the efficiency of the patch repair, the sharp stress concentration at the crack tip should be removed. Drilling a hole at the crack tip before patching increases the resistance to crack growth under an applied load. Damage to the specimen is stopped altogether by using a combination

of drilling holes at the crack tips and patching. When the stop holes are filled with a plug material, the repair has the ability to retain pressure and resist biaxial loading.

5.3   PATCH DESIGN PROTOCOL

Design of the patch occurs in two stages. Initially, the patch should be designed so that no component of the patched assembly fails under an applied load. This first stage ensures that the static strength required of the bonded assembly is met by both the composite patch and the adhesive bond. Next, the patched assembly must be designed so that the patch is effective in repairing the damaged steel assembly. Thus, the effect of the patch on damage in the steel pressure vessel must be understood.

5.3.1   Strength of the Patch and Adhesive Bond

The following protocol is useful in designing the carbon fibre composite patch so that it will meet the strength requirements imposed by the applied load:

i)   *The patch should not fail*

In a damaged pressure vessel with a bonded patch, the applied load is going to be supported by the bonded patch.

ii)   *The bond should not fail*

The amount of load transferred to the patch should not exceed the amount of load which the adhesive bond can transfer. This means that the surface of the steel pressure vessel should be adequately cleaned and treated for bonding and that the overlap length of the patch on the steel structure is designed to be

long enough to transfer the load efficiently. For a sandblasted steel surface bonded and cured at 93°C (200°F), the ultimate load per unit width that the specimen can withstand is 920 kN/m (5250lb/in).

iii)   **The patch should not be designed so that the bond will fail**

At this point, it should be checked that the composite patch or the adhesive bond will not fail under loading of the pressure vessel. If either of the components are deemed to fail, the patch design or the selected adhesive should be changed. Altering the direction of the fibres in the composite patch or the thickness of the composite patch will alter the strength and tensile stiffness of the patch, thus, altering the load which is carried by the patch. Altering the adhesive properties or the adhesive bond overlap length will alter the ability of the adhesive bond to transfer this load to the patch. An iterative process to determine the patch and adhesive design is required to meet the strength requirements for both.

5.3.2   Effectiveness of the Patch and the Adhesive Bond

Having a strong patch and adhesive bond is not sufficient. The repair design must also be effective at prolonging the life of the damaged pressure vessel significantly.

5.4   PRACTICAL DESIGN CONSIDERATIONS TO BE INVESTIGATED

1)   The CT specimens tested did not last more than 500 hours before failure. In a practical patching application, however, the patch would need to be employed for periods of time extending weeks or even months. Creep of the epoxy under an applied mean load would become a design consideration and

should be investigated.

2)   The effect of higher temperature or corrosive environment on the material properties of the composite patch and adhesive layer are not known. Hukaluk et al [5.1] observed that when tested at 100°C and 100% RH, carbon fibre patches bonded to aluminum using a room-temperature curing adhesive debonded fully during a cyclic load application. Parker [5.2] also found that joint strength can be directly related to the moisture content of the adhesive layer. During the operating life of a pressure vessel, damaging fluids such as water, various petrochemicals, or solar radiation can effect the quality of the bond.

3)   The thickness of the adhesive layer affects the stress and strain gradients in the adhesive layer.

4)   The material properties of the adhesive affect both the amount of load that can be transferred from the crack steel structure to the patch and the resistance of the patched assembly to debonding. The selection of a strong durable adhesive with minimum temperature cure would be advantageous for the repair.

5)   The size of the hole to be drilled at crack tip is correlated to the stress intensity at this point. A larger hole would produce less of a stress concentration but would be harder to plug to maintain pressure in a pressure vessel application.

6)   The plug used in this investigation was a tin-lead solder material. In a practical pressure vessel application, it would be better to use a stronger filler material.

7)   The patch applied in these applications was applied under a no-load condition. In practical applications, it would be desirable to apply the patch when the pressure vessel is still in operation. The effectiveness of a patch applied to a pressure vessel under load needs to be investigated.

8)   The patch used in this investigation is a carbon fibre composite material. Using a material with a higher tensile stiffness would be better at both transferring load away from the cracked structure and bridging the crack.

5.5   REFERENCES

[5.1]   Hukaluk, P., Raizenne, M.D., and Scott, R.F., *"Influences of Environment and Stress History on the Composite Patch Repair of Cracked Metallic Structures"*, Canadian Aeronautics and Space Journal, Vol. 34, No. 2, June, 1988, pp. 85-91.

[5.2]   Parker, B.M., *"The Durability of Adhesive Bonded Epoxy Carbon Fibre Composites"*, Composite Bonding, ASTM STP 1227, D.S. Damico, T.L. Wilkinson, Jr., and S.L.F. Niks (ed.), American Society for Testing and Materials, 1994, pp.68-81.

Appendix A: Calculating Crack Growth Rate, da/dN.

The rate of the crack growth, *da/dN*, is determined from the crack length ratio, *a/w*, verses the elapsed cycles, N, data. The four methods described below were used to calculate *da/dN* and the results are compared.

Method #1:

Method #1 used the method recommended by the ASTM standard [A.1] on crack growth calculation.

1. From the experimental data of the normalized potential drop, P/Po, verses the number of cycles, a P/Po reading was extrapolated every 100,000 cycles. This insured that the minimum requirement for crack growth between data points, $\Delta a > 0.25$mm, was achieved.

2. The selected P/Po data was converted to a crack length ratio, *a/w*, using the calibration equation 4.2.

3. Using the *a/w* verses the number of cycles data, the growth rate was calculated using the Incremental Polynomial Method. The Incremental Polynomial Method involves fitting a second order polynomial to sets of successive data points.

4. The growth rate was obtained from the derivative of the above polynomials.

Method #2:

1. The P/Po data was converted to *a/w* using the calibration equation 4.2.

2. The relation of the crack growth ratio, *a/w*, to the number of cycles, N, was fit using an 8th degree polynomial.

3. The growth rate was determined by applying the secant method to the fitted *a/w* data:

$$(da/dN)_i = (a_{i+1} - a_{i-1})/(N_{i+1} - N_{i-1}).$$

94

Method #3:

1. The P/Po data was converted to a/w using the calibration equation 4.2.

2. The relation of the crack growth ratio, a/w, to the number of cycles was fit using 4 second order polynomials.

3. The growth rate was determined using the secant method.

Method #4:

1. P/Po was converted to a/w using the calibration equation 4.2.

2. The relation of the crack growth ratio, a/w, to the number of cycles, N, was fit using an 8th degree polynomial.

3. From the crack ratio data, an a/w data point was extrapolated every 100,000 cycles.

4. The growth rate was determined using the secant method.

Figures A.1-A.4 show the crack growth rate, da/dN, as a function of the crack length ratio, a/w, calculated using the four methods described above. The figures illustrate that the calculation of the crack growth rate, da/dN, is generally independent of the method used. For this reason, and because Method #2 was the easiest to employ, Method #2 was used to calculate the crack growth rate for both the patched and the unpatched CT propagation specimens.

REFERENCES

[A.1] ASTM Designation E647-91, "Standard Test Method for Measurement of Fatigue Crack Growth Rates".
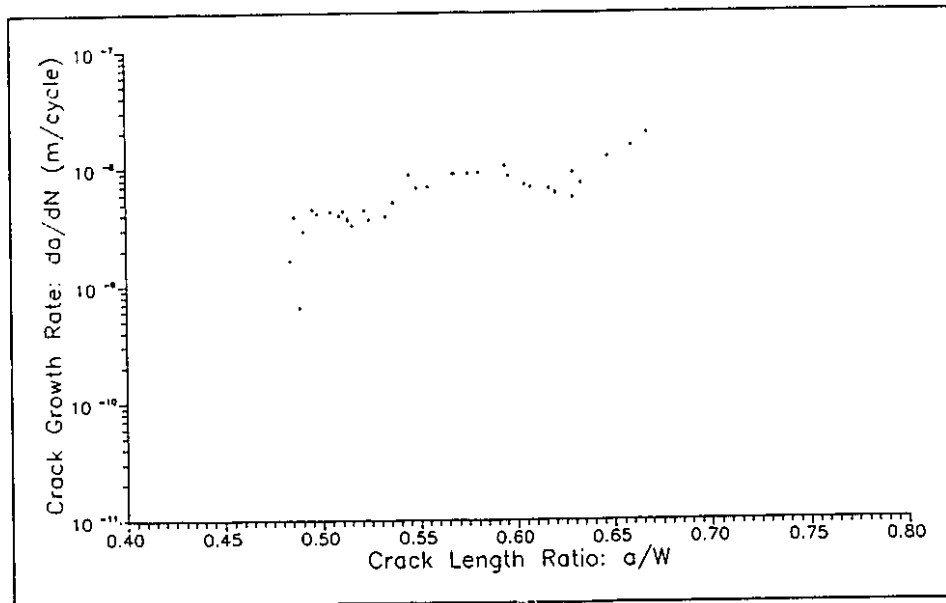
Appendix A: Calculating Crack Growth Rate, da/dN.

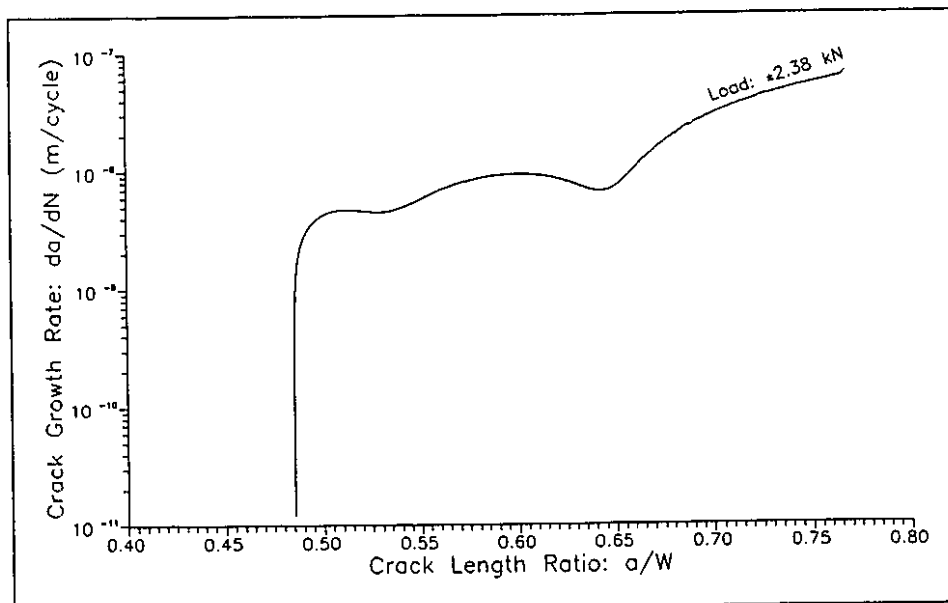Figure A.1: Growth rate, *da/dN*, calculated using Method #1.

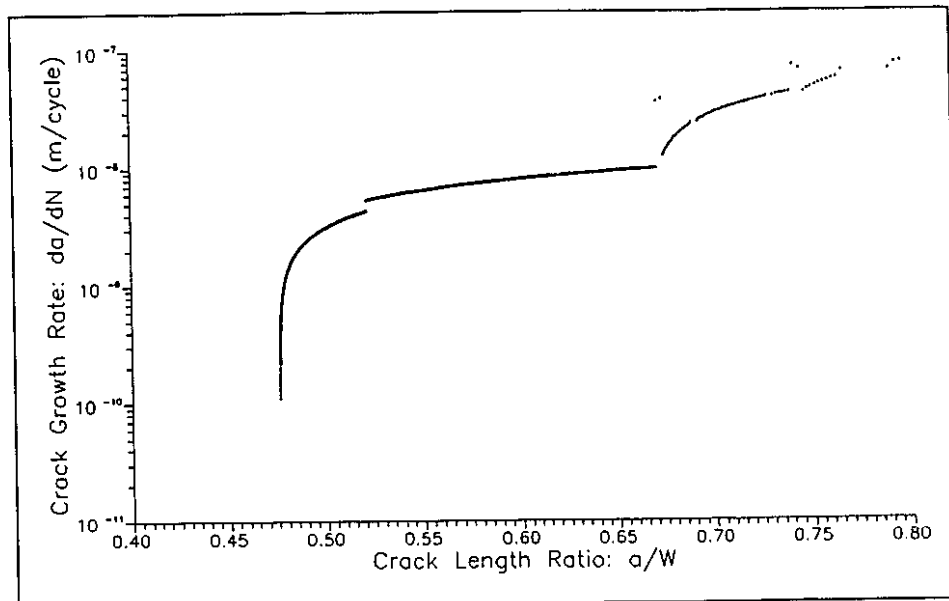Figure A.2: Growth rate, *da/dN*, calculated using Method #2.
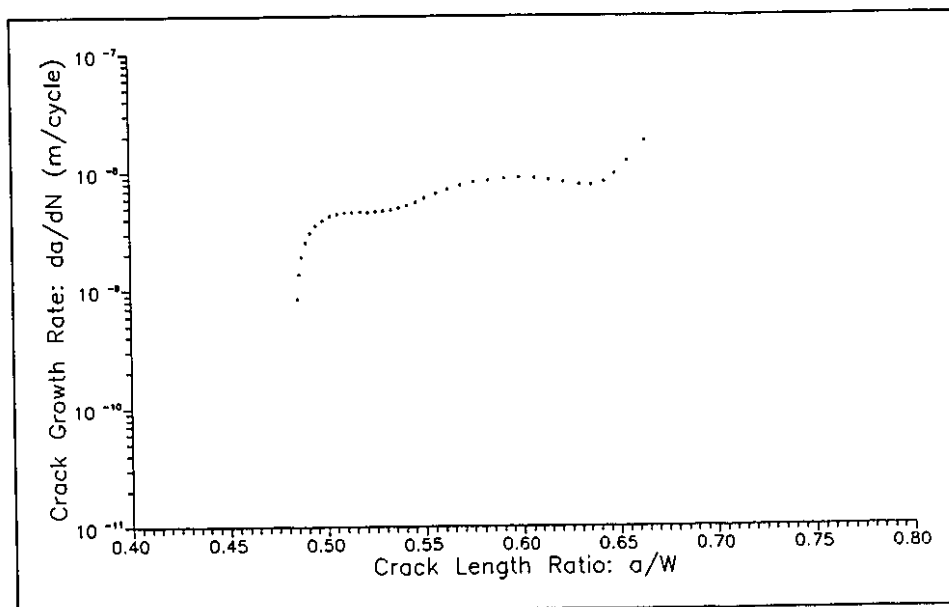
Figure A.3: Growth rate, *da/dN*, calculated using Method #3.

Figure A.4: Growth rate, *da/dN*, calculated using Method #4.